CrystEngComm

Accepted Manuscript

This article can be cited before page numbers have been issued, to do this please use: W. X. Oliveira, W. D. do Pim, C. B. Pinheiro, Y. Journaux, M. Julve and C. L. M. Pereira, *CrystEngComm*, 2019, DOI: 10.1039/C9CE00215D.

ROYAL SOCIETY OF CHEMISTRY

rsc.li/crystengcomm

View Article Online
DOI: 10.1039/C9CE00215D

Monitoring the hydrogen bond net configuration and the dimensionality of aniline and phenyloxamate by adding 1*H*-pyrazole and isoxazole as substituents for molecular self-recognition

Willian X. C. Oliveira,[†] Walace D. do Pim, [‡] Carlos B. Pinheiro,[§] Yves Journaux,[⊥] Miguel Julve[‖] and Cynthia L. M. Pereira*[,†]

[†]Departamento de Química, Instituto de Ciências Exatas, Universidade Federal de Minas Gerais. Av. Pres. Antônio Carlos, 6620, Pampulha, 31270-901 Belo Horizonte, Minas Gerais, Brazil;

[‡]Centro Federal de Educação Tecnológica de Minas Gerais, Av. Amazonas, 5253, Nova Suíça, 30421-169 Belo Horizonte, Minas Gerais, Brazil.

[§]Departamento de Física, Instituto de Ciências Exatas, Universidade Federal de Minas Gerais. Av. Pres. Antônio Carlos, 6620, Pampulha, 31270-901 Belo Horizonte, Minas Gerais, Brasil;

[⊥] Sorbonne Université, CNRS, Institut Parisien de Chimie Moléculaire, IPCM, 75005, Paris, France.

[‖]Instituto de Ciencia Molecular (ICMol), Universitat de València, C/ Catedrático José Beltrán 2, 46980 Paterna, València, Spain.

*Corresponding author e-mail: cynthialopes@ufmg.br

View Article Online
DOI: 10.1039/C9CE00215D

Abstract

This work describes the synthesis and characterization of a new class of oxamic acid derivatives containing pyrazole and isoxazole as substituents to investigate their ability to form hydrogens bonds aiming at applying them in crystal engineering and molecular self-recognition. In this respect, we report a new synthesis of 2-(4-nitrophenyl)-1,3-propanedial (**1**) in a high yield using $SOCl_2$ as chlorinating agent. The new oxamic esters 4-(1*H*-pyrazol-4-yl)phenylene-*N*-(ethyloxamate) (**2d**) and 4-(1,2-oxazol-4-yl)phenylene-*N*-(ethyloxamate) (**3d**) were prepared from **1**. The synthetic route consists of the cyclisation of **1** either with hydrazine to afford the 4-(-aminophenyl)-1*H*-pyrazole (**2a**) or with hydroxylamine to obtain the isozaxole-based molecule 4-(4-nitrophenyl)-1,2-oxazole (**3a**). The reduction of **2a** and **3a** was carried out in an acidic/tin solution to yield 4-(4-ammoniophenyl)-1*H*-pyrazol-2-ium trichlorostannate(II) chloride monohydrate (**2b**) and 4-(4-ammoniophenyl)-1,2-oxazole hexachlorostannate(IV) (**3b**). Basic extraction of **3b** provided 4-(4-aminophenyl)-1,2-oxazole (**3c**). The reduction of **2a** to 4-(4-aminophenyl)-1*H*-pyrazole (**2c**) was achieved by means of hydrazine associated to supported palladium on carbon. The condensation of **2c** and **3c** with ethyl chlorooxoacetate delivers oxamic esters **2d** and **3d**. In *n*-tetrabutylammonium hydroxide solution **2d** is fully hydrolyzed, obtaining the *n*-tetrabutylammonium salt of 4-(1*H*-pyrazole-4-yl)phenylene-*N*-oxamate as hemihydrate (**2e**). The low stability of isoxazole molecules in basic solutions was proved by crystallizing the *n*-tetrabutylammonium salt of 1-cyano-1-(4-nitrophenyl)-2-oxoethanide (**3f**) (obtained by cleavage of **3d** with *n*-Bu_4NOH) and preparing its conjugated acid 2-(4-nitrophenyl-3-oxopropanenitrile (**3e**). The structures of **2b**, **3b**, **3d** and **2e** were solved by single crystal X-ray diffraction techniques. The analysis of their crystal packing reveals hydrogen bond features compatible for all compounds as well as some differences depending on the pH of the crystallization solution and the presence or absence of the oxamate group due to the increase of hydrogen bond donors and acceptors.

Introduction

The specific interaction of a group, molecule or even an ion with other group in the same molecule or another one is referred to as molecular recognition.[1-3] The specific recognition of molecules are very relevant as shown by biomolecular chemistry because it rules the living organisms. Proteins and other receptors have specific interactions in the voids that must be fulfilled in order to recognize a target molecule.[4-6] Among the interactions involved in these processes, we will focus on the hydrogen bonds since they are in general directional and due to the stability they afford to the system, they can rule the spatial structure of the molecule, adduct, synthon or even of the whole crystal packing. The most famous example of hydrogen bond controlling the structure in biology is the DNA double helix, where the interaction between the nitrogenous bases links the strands and together with the phosphate-sugar backbone leads to the helicoidal structure of the macromolecule, which is so strong that only the replication enzymes can break it.[4] In this respect, the molecular recognition for small molecules can be a ruler for the crystal engineering and it certainly deserves deeper studies and understanding.

In terms of crystal engineering, the molecular recognition allows the user to guide the self-assembly of the basic units leading to better planning of the supramolecular structures and consequently, to modulate the properties which are dependent on the specific organization in the space.[7-11] In order to reach the molecular recognition and crystal engineering, one must rely on supramolecular chemistry, the science field dealing with the study of the interactions among particles, since all interactions are relevant during the crystallization process, hydrogen bonding being one of them. One can state that the stronger the interaction, the more relevant for the crystallization it is, [7,11] and so, the hydrogen bonds may be the focus of crystal engineering. Finally, a smart way to modulate the crystallization would be the introduction of hydrogen bonds donors/acceptors in specific parts of the molecule, just as nature has done in DNA.

Given that the 1*H*-pyrazole groups (a member of the azole family)[12,13] (Chart 1) is known to be hydrogen bond donor and acceptors, its insertion into molecules can turn it capable of molecular recognition or even self-recognizable.[14-25] The pyrazole-nitrogen atoms have double functions because the protonated one is responsible for recognizing electronegative atoms

View Article Online
DOI: 10.1039/C9CE00215D

whereas the tertiary one can be recognized by hydrogen bond donor groups. This duality can culminate in a variety of self-recognition hydrogen bonded nets: discrete supramolecules[14-22] or supramolecular polymers,[23-25] as displayed in Chart 2.

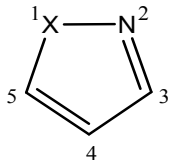

Chart 1. General structure of the 1,2-azole group: 1*H*-pyrazole (X = N-H) and isoxazole (X = O).

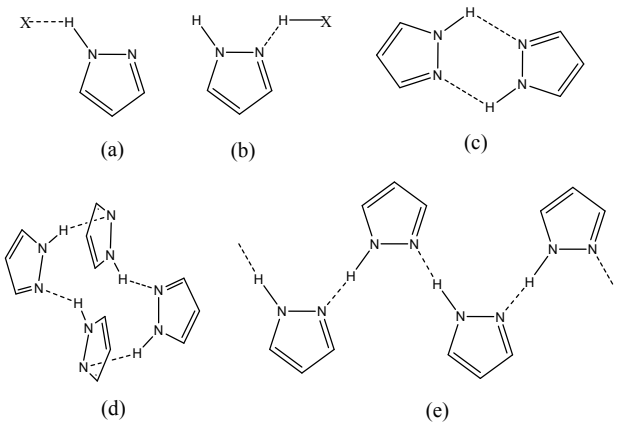

Chart 2. Common hydrogen bonds and supramolecular motifs in 1*H*-pyrazole-based assemblies: recognition of (a) an electronegative group and (b) an electrodeficient hydrogenated group; (c) discrete dimeric, (d) tetrameric and (e) linear chain self-recognition.

On the other hand, the isoxazole group is formed by placing an oxygen atom at one position distinct from the nitrogen in the azole ring. This member of the azole family is not capable of molecular recognition in the same way as the 1*H*-pyrazole due to the lack of a hydrogen bond donor. Isoxazole groups in presence of hydrogen donor molecules only interact with them through their nitrogen atom because the isoxazole-oxygen atom is heavily electronegative and its electron density is unavailable to interact.[13] Then, this group can be used for comparison of the importance of a protonated group in the self-assembly concerning the pyrazole-based molecules.

View Article Online
DOI: 10.1039/C9CE00215D

This work describes the synthesis of new class of oxamate based-molecules as molecular recognition agents based on the control of hydrogen bond networks, taking into consideration the interaction between the pyrazole- and isoxazole substituted molecules and non-substituted aniline and phenyloxamate molecules.

Experimental Section

All crude materials were purchased from commercial sources and used as received. The solvents dmf and thf were dried over molecular sieves. Tetra-*n*-butylammonium hydroxide 40% aqueous solution was used in the preparations. The synthetic routes of the pyrazole- and isoxazole-substituted oxamates are shown in Schemes 1 and 2, respectively.

2-(4-nitrophenyl)-1,3-propanedial (1). $SOCl_2$ (3.20 mL, 60.0 mmol) was introduced into a round flask which was cooled in an ice bath (between 0 and 4 ºC); then, dried dmf (7.30 mL, 100 mmol) was slowly added, under vigorous stirring, in order to maintain the temperature below 4 ºC. After completing the addition of dmf, the solution was kept to react under 30 min when solid 4-nitrophenylacetic acid (3.60 g, 20.0 mmol) was added. The mixture was heated up to 90 ºC, kept at this temperature for 6 h and allowed to cool down to room temperature. The round flask was placed again in an ice bath and cold water (below 4 ºC) was added (130 mL) to it followed by the careful addition a cold aqueous solution of NaOH (30 mL, 10 mol L^{-1}). This mixture was left overnight under stirring at room temperature, then heated up again at 115 ºC for 4 h and allowed to cool down at room temperature. The resulting bright red solid which was formed, was filtered off, dissolved in water (250 mL) and filtered to remove a small amount of black byproduct. This final mother liquor was acidified with concentrated HCl until pH 1.0 and a pale-yellow solid was separated. This yellow product was filtered off, washed with water and left to dry under low pressure for 24 h. Yield: 65% (2.51 g, 13.0 mmol). ^{1}H NMR (dmso-d_6, 200 MHz): 7.85 (d, 2H, J = 9.0 Hz, **H**-ph), 8.21 (d, 2H, J = 9.0 Hz, **H**-Ph), 8.65 (s, 2H, COC**H**CO) ppm. ^{13}C NMR (dmso-d_6, 50 MHz): 118.69, 123.16, 130.06, 139.29, 145.78, 181.17 ppm. Elemental

analysis for $C_9H_7NO_4$ (**1**) [Exp. (Calcd.)]: C 56.52 (55.96), H 2.81 (3.05), N 7.00 (7.25)%. Melting point: 230-232 ºC (followed by decomposition).

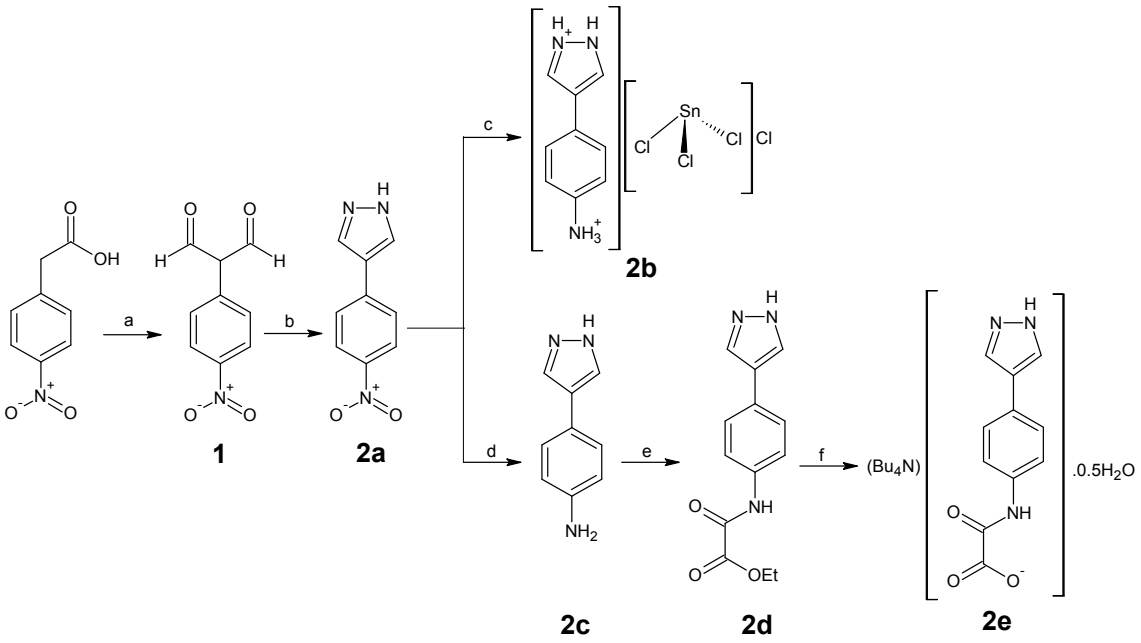

Scheme 1. Synthetic pathway of the pyrazole derivatives from **1**. (a) $SOCl_2$, dmf, 90 ºC for 6 h; NaOH, 120 ºC for 3 h; HCl. (b) $NH_2NH_2{\cdot}H_2O$, MeOH, 100 ºC for 3 h. (c) Sn, HCl; EtOH and slow cooling. (d) $NH_2NH_2{\cdot}H_2O$, Pd/C, MeOH, for 1 h. (e) ClC(O)COOEt, Et_3N, thf, 75 ºC for 1h. (f) *n*-Bu_4NOH_{aq}.

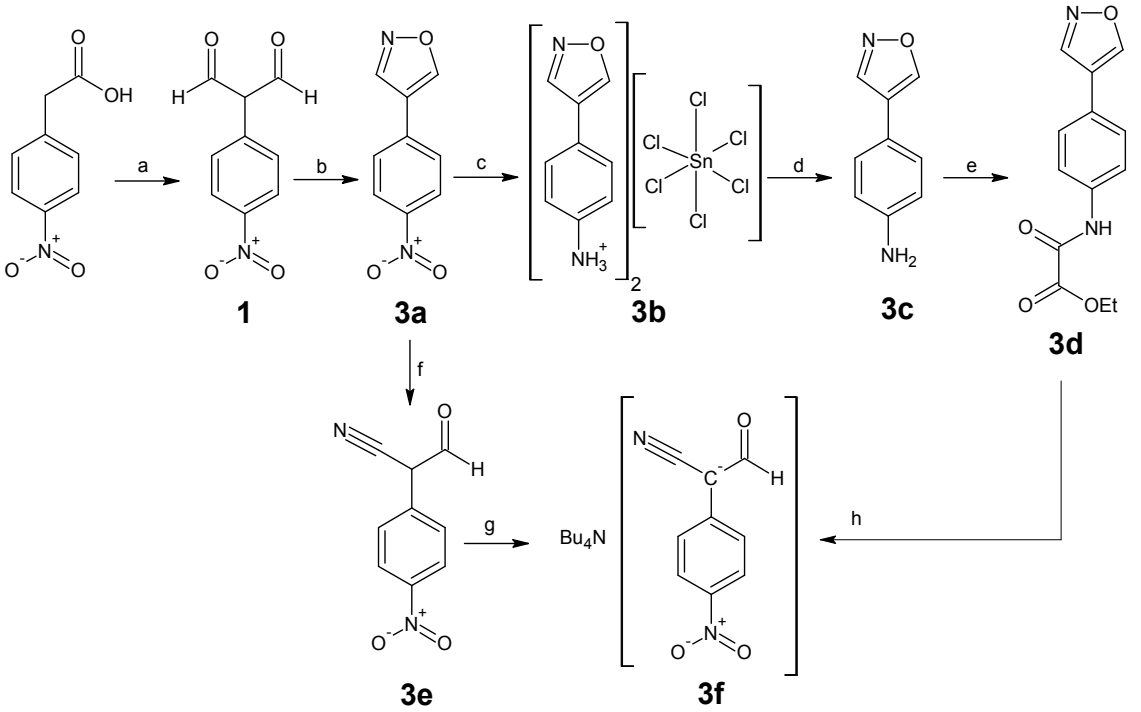

Scheme 2. Synthetic pathway of isoxazole derivatives from 2-(4-nitrofenil)-1,3-propanedial (**1**).

View Article Online
DOI: 10.1039/C9CE00215D

(a) $SOCl_2$, dmf, 90 ºC for 6 h; NaOH, 120 ºC for 3 h; HCl. (b) NH_3OHCl, MeOH, 100 ºC for 3 h. (c) Sn, HCl; EtOH and slow cooling. (d) $NaCO_3$, extraction with $CHCl_3$. (e) ClC(O)COOEt, Et_3N, thf, 75 ºC for one hour. (f) KOH, CH_3OH, 90 ºC for 2 h; HCl 1.0 M. (g) and (h) *n*-Bu_4NOH_{aq}.

4-(4-nitrophenyl)-1*H*-pyrazole (2a). Hydrazine monohydrate (0.385 mL, 5.28 mmol) and methanol (20.0 mL) were poured into a round flask containing a solid sample of **1** (1.00 g, 5.28 mmol) and the mixture was allowed to react at 100 ºC for 3 h. Then, water (20.0 mL) was added and the temperature was kept until complete dissolution. Slow cooling of this solution at room temperature afforded a crystalline yellowish-orange solid which was filtered off, washed with water and left to dry under low pressure for 24 hours. Yield: 67% (669 mg, 3.54 mmol). ^{1}H NMR (dmso-d_6, 200 MHz): 7.92 (d, 2H, *J* = 8.6 Hz, **H**-Ph), 8.21 (m, 3H, **H**-Ph + **H**-pyrazole), 8.49 (s, 1H, **H**-pyrazole), 13.28 (s, 1H, N**H**-pyrazole) ppm. ^{13}C NMR (dmso-d_6, 50 2a MHz): 119.81, 124.61, 128.88, 137.54, 140.53, 145.36 ppm. Elemental analysis for $C_9H_7N_3O_2$ (**2a**) [Exp. (Calcd.)]: C 57.98 (57.14), H 2.84 (3.03), N 22.12 (22.21)%. Melting point: 200-202 ºC.

4-(4-ammoniophenyl)-1*H*-pyrazole-2-ium trichlorostannate(II) chloride monohydrate (2b). Granulated tin (200 mg, 1.68 mmol) and concentrated HCl (4.0 mL) were poured into a round flask containing solid **2a** (100 mg, 0.53 mmol) and the whole was kept under continuous stirring at 130 ºC until a clear colorless solution was reached. After the color change, ethanol (4.0 mL) was added and the resulting solution was allowed to cool down at room temperature. The white crystalline solid that separated was collected by filtration, washed with cold ethanol and diethyl ether and left to dry under ambient conditions for 24 hours. Elemental analysis for $C_9H_{13}Cl_4N_3OSn$ (**2b**) [Exp. (Calcd.)]: C 24.02 (23.11), H 2.05 (1.94), N 8.97 (8.98), Sn 26.58 (25.38)%. ^{1}H NMR (dmso-d_6, 200 MHz): 7.42 (d, 2H, *J* = 8.4 Hz, **H**-Ph), 7.76 (d, 2H, *J* = 8.4 Hz, **H**-Ph), 8.24 (s, 2H, **H**-pyrazolium), 10.21 (s, 5H, **H**N–N**H**-pyrazolium + N**H**$_3$-anilinium) ppm. ^{13}C NMR (dmso-d_6, 50 MHz): 122.07, 125.56, 127.97, 131.20, 132.79, 134.22 ppm.

4-(4-aminophenyl)-1*H*-pyrazole (2c). Hydrazine monohydrate (0.800 mL, 20.0 mmol), palladium on carbon (500 mg, 10% w/w) and methanol (40.0 mL) were added to a round flask containing solid **2a** (1.00 g, 5.26 mmol). The mixture was left to react at 100 ºC under continuous

View Article Online
DOI: 10.1039/C9CE00215D

stirring for 3 h. The resulting suspension was filtered off to remove the carbon and the mother liquor was evaporated to one fifth of the initial volume for precipitation of a bright white solid. This product was collected by filtration, washed with cold methanol (1.0 mL) and dried under low pressure for 24 hours. Yield: 75% (628 mg, 3.94 mmol). ^{1}H NMR (dmso-d_6, 200 MHz): 4.99 (s, 2H, N**H**$_2$), 6.57 (d, 2H, *J* = 9.6 Hz, **H**-Ph), 7.26 (d, 2H, *J* = 10.0 Hz, **H**-Ph), 7.83 (s, 2H, **H**-pyrazole), 12.71 (s, 1H, N**H**-pyrazole) ppm. ^{13}C NMR (dmso-d_6, 50 MHz): 114.62, 121.06, 122.29, 126.33, 135.38, 147.25 ppm. Elemental analysis for $C_9H_9N_3O$ (**2c**) [Exp. (Calcd.)]: C 67.44 (67.90), H 5.57 (5.70), N 26.27 (26.40)%. Melting point: 232-234 ºC.

4-(1*H*-pyrazole-4-yl)phenylene-*N*-(ethyloxamate) (2d). Solid **2c** (1.04 g, 6.6 mmol) was introduced into a round flask containing thf (200 mL) and trimethylamine (0.93 mL, 6.7 mmol). Ethyl chlorooxoacetate (0.75 mL, 6.6 mL) dissolved in diethyl ether (10.0 mL) was slowly added to the previous solution under continuous stirring. The final mixture was allowed to react for 1 h at 75 ºC. Then, the solution was evaporated to one fifth of the initial volume and the further addition of cold water (200 mL) caused the precipitation of a white polycrystalline solid. This precipitate was collected by filtration, washed with water and dried at low pressure for 24 h. Yield: 86% (1.47 g, 5.68 mmol). Elemental analysis for $C_{13}H_{13}N_3O_3$ (**2d**) [Exp. (Calcd.)]: C 59.98 (60.22), H 4.88 (5.05), N 16.17 (16.21)%. ^{1}H NMR (dmso-d_6, 200 MHz): 1.32 (t, 3H, *J* = 7.1 Hz, OCH$_2$C**H**$_3$), 4.31 (q, 2H, *J* = 7.1 Hz, OC**H**$_2$CH$_3$), 7.59 (d, 2H, *J* = 8.6 Hz, **H**-Ph), 7.73 (d, 2H, *J* = 8.7 Hz, **H**-Ph), 10.78 (s, 2H, N**H**-oxamate) ppm. ^{13}C NMR (dmso-d_6, 50 MHz): 14.22, 62.72, 121.16, 125.69, 129.87, 135.68, 155.66, 161.06 ppm. Melting point: 230-232 ºC.

Tetra-*n*-buthylammonium 4-(1*H*-pyrazole-4-yl)phenylene-*N*-oxamate hemihydrate (2e). Solid **2d** (260 mg, 1.00 mmol), tetra-*n*-buthylammonium hydroxide (0.655 mL, 1.01 mmol) and water (10.0 mL) were introduced into to a round flask and the resulting suspension was left to react under continuous stirring at 80 ºC for one hour. Then, it was allowed to cool down at room temperature and colorless plates as its characteristic external shape that separated were collected by filtration washed with water and left to dry on filter paper in the open air for 24 h. Yield: 88% (417 mg, 0.88 mmol). Elemental analysis $C_{27}H_{45}N_4O_{3.5}$ (**2e**) [Exp. (Calcd.)]: C 67.21 (67.19), H 8.99 (9.19), N 8.78 (8.71)%. ^{1}H NMR (dmso-d_6, 300 MHz): 0.93 (t, 12H, *J* = 7.3 Hz,

View Article Online
DOI: 10.1039/C9CE00215D

$NCH_2CH_2CH_2C\mathbf{H}_3$), 1.30 (m, 8H, $NCH_2CH_2C\mathbf{H}_2CH_3$), 1.56 (m, 8H, $NCH_2C\mathbf{H}_2CH_2CH_3$), 3.16 (m, 8H, $NC\mathbf{H}_2CH_2CH_2CH_3$), 7.49 (d, 2H, J = 8.5 Hz, **H**-Ph), 7.70 (d, 2H, J = 8.5 Hz, **H**-Ph), 7.97 (s, 2H, **H**-pyrazole), 10.00 (s, 1H, N**H**-pyrazole), 12.88 (s, 1H, N**H**-oxamate) ppm. ^{13}C NMR (dmso-d_6, 75 MHz): 13.84, 19.56, 23.42, 57.88, 119.40, 121.46, 125.61, 127.73, 137.61, 162.87, 164.93 ppm. Melting point: 238-239 ºC.

4-(4-nitrophenyl)-1,2-oxazole (3a). Solid **1** (1.00 g, 5.28 mmol) was introduced into a round flask containing hydroxylamine hydrochloride (400 mg, 2.87 mmol) and methanol (20.0 mL). This mixture was left to react under continuous stirring at 100 ºC for 3h. Then, water (20.0 mL) was added and the temperature was kept until the complete dissolution of the solid. Slow cooling of this solution afforded a crystalline orange solid which was filtered off, washed with water and left to dry under low pressure for 24 h. Yield: 75% (752 mg, 3.96 mmol). Elemental analysis for $C_9H_6N_2O_3$ (**3a**) [Exp. (Calcd.)]: C 56.81 (56.85), H 3.22 (3.18), N 14.55 (14.73)%. ^{1}H NMR (dmso-d_6, 200 MHz): 7.76 (d, 2H, J = 9.0 Hz, **H**-Ph), 8.19 (d, 2H, J = 8.9 Hz, **H**-Ph), 8.81 (s, 1H, **H**-isoxazole), 9.15 (s, 1H, **H**-isoxazole) ppm. ^{13}C NMR (dmso-d_6, 50 MHz): 120.46, 125.24, 128.02, 136.31, 147.85, 148.61, 156.84 ppm. Melting point: 166-168 ºC.

Bis-4-(4-ammoniophenyl)-1,2-oxazole hexachlorostannate(IV) (3b). Granulated tin (200 mg 1.68 mmol) and concentrated HCl (4.0 mL) were poured into a round flask containing solid **3a** (100 mg; 0.53 mmol). The whole mixture was heated at 130 ºC under continuous stirring until a clear pale-yellow solution was reached. After the color change, ethanol (4.0 mL) was added and left the solution to cool down slowly. The yellow crystalline solid which was formed was collected by filtration, washed with cold ethanol (1.0 mL) and diethyl ether (3.0 mL) and left to dry under ambient conditions for 24 h. Yield: 65% (225 mg, 0.34 mmol). Elemental analysis for $C_{18}H_{18}Cl_6N_4O_2Sn$ (**3b**) [Exp. (Calcd.)]: C 32.28 (32.97), H 2.87 (3.07), **N** 8.12 (8.54), Sn 18.07 (18.16)%. ^{1}H NMR (dmso-d_6, 200 MHz): 7.39 (d, 2H, J = 8.5 Hz, **H**-Ph), 7.78 (d, 2H, J = 8.7 Hz, **H**-Ph), 9.17(s, 1H, **H**-isoxazole), 9.47(s, 1H, **H**-isoxazole) ppm. ^{13}C NMR (dmso-d_6, 50 MHz): 121.55, 124.93, 129.15, 134.15, 149.90, 157.01 ppm.

View Article Online
DOI: 10.1039/C9CE00215D

4-(4-aminophenyl)-1,2-oxazole (3c). Solid **3b** (1.00 g 1.52 mmol) was added to an aqueous solution (10.0 mL) of sodium carbonate (0.5 g 4.25 mmol) in a round flask. This mixture was left to react under continuous stirring for 30 min at room temperature and the title compound was extracted with two portions of chloroform (20 mL). The organic phases were combined and evaporated until dryness to afford a yellow solid. Yield: 95% (487 mg, 3.04 mmol). Elemental analysis for $C_9H_8N_2O$ (**3c**) [Exp. (Calc.)]: C 67.55 (67.49), H 5.00 (5.03), N 17.22 (17.49)%. ^{1}H NMR (dmso-d_6, 300 MHz): 5.26 (s, 2H, N**H**$_2$), 6.63 (dd, 2H, *J* = 8.5 Hz, *J'* = 1.9 Hz, **H**-Ph), 7.36 (dd, 2H, *J* = 8.5 Hz, *J'* = 1.9 Hz, **H**-Ph), 8.97 (s, 1H, **H**-isoxazonium), 9,16 (s, 1H, **H**-isoxazonium) ppm. ^{13}C NMR (dmso-d_6, 75 MHz): 114.49, 115.89, 121.68, 127.46, 148.35 148.86, 152.80 ppm. Melting point: 311 ºC (decomp.).

4-(1,2-oxazol-4-yl)phenylene-*N*-(ethyloxamate) (3d). Solid **3c** (1.04 g, 6.6 mmol), trimethylamine (0.93 mL, 6.7 mmol) and thf (200 mL) were introduced into a round flask. Diethyl ether (10.0 mL) containing ethyl chloroacetate (0.75 mL, 6.6 mL) and was slowly added added to the resulting solution under continuous stirring and the mixture was allowed to react for one hour at 75 ºC. Then, the volume was reduced to one fifth and cold water (200 mL) was added to precipitate a pale-yellow crystalline solid. It was collected by filtration, washed with water and dried at low pressure for 24 h. Yield: 86% (1.47 g, 5.68 mmol). Elemental analysis for $C_{13}H_{12}N_2O_4$ (**3d**) [Exp. (Calcd.)]: C 60.02 (60.00), H 4.88 (4.65), **N** 10.58 (10.76)%. ^{1}H NMR (dmso-d_6, 300 MHz): 1.32 (t, 3H, *J* = 7.1 Hz, OCH$_2$C**H**$_3$), 4.31 (q, 2H, *J* = 7.1 Hz, OC**H**$_2$CH$_3$), 7.59 (dd, 2H, *J* = 8.7 Hz, *J'* = 2.0 Hz, **H**-ph), 7.73 (dd, 2H, *J* = 8.8 Hz, *J'* = 1.9 Hz, **H**-ph), 10.78 (s, 2H, N**H**-oxamate) ppm. ^{13}C NMR (dmso-d_6, 75 MHz): 14.22, 62.72, 121.16, 125.69, 129.87, 135.68, 155.66, 161.06 ppm. Melting point: 210-212 ºC. In order to crystallize this product, **3d** (10 mg) dissolved in dmso (0.5 mL) was deposited at the bottom of a test tube (4.0 mL) and the tube was filled with a water:dmso solvent mixture (3.0 mL, 50% v/v). The tube was covered with Parafilm® and pale-yellow plates were grown on standing at room temperature after two weeks. They were collected by filtration, washed with water and dried at low pressure for 24 hours. Yield: 75% (7.5 mg).

View Article Online
DOI: 10.1039/C9CE00215D

2-(4-nitrophenyl)-3-oxopropanenitrile (3e). Solid **3a** (350 mg, 1.84 mmol) was allowed to react with an aqueous solution (20 mL) of KOH (400 mg, 8.40 mmol) in a round flask under continuous stirring for 24 h at room temperature. The solution was filtered to discard any small particle and concentrated HCl was poured into it until reaching a pH value of 1.0. The yellow solid which was formed, was filtered off, washed with water and left to dry at low pressure for 72 h. Yield: 58% (203 mg, 1.06 mmol). Elemental analysis for $C_9H_6N_2O_3$ (**3e**) [Exp. (Calcd.)]: C 58.02 (56.85), H 3.38 (3.18), N 14.58 (14.73). ^{1}H NMR (CD_3CN, 100 MHz): 4.01 (s, 1H, HC(O)C**H**CN), 7.63 (d, 4H, J = 9.0 Hz, **H**-Ph), 7.72 (s, 1H, **H**C(O)CHCN), 7.96 (d, 2H, J = 9.1 Hz, **H**-Ph), 8.07 (s, 2H, **H**C(OH)CCN), 8.22 (m, 6H, **H**-Ph) ppm. ^{13}C NMR (CD_3CN, 100 MHz): 123.77, 124.03, 124.20, 124.79, 127.53, 129.28, 139.27, 159.68, 161.01 ppm. Melting point: 235-238 (dec.) ºC.

Tetra-*n*-butylammonium 1-cyano-1-(4-nitrophenyl)-2-oxoethanide (3f). Solid **3e** (50.0 mg, 0.263 mmol) was added to a mixture of tetra-*n*-butylammonium hydroxide 40% aqueous solution (200 µL, 0.307 mmol) and water (5.0 mL) in a beaker. The whole was left to react in an ultrasound bath to achieve a suspension of a red powder. This powder was filtered off, washed with water and left to dry at low pressure for 72 hours. Yield: 97% (110 mg, 0.255 mmol). Elemental analysis for $C_{25}H_{41}N_3O_3$ (**3f**) [Exp. (Calc.)]: C 69.49 (69.57), H 9.79 (9.57), N 9.71 (9.74)%. ^{1}H NMR ($CDCl_3$, 400 MHz): 0.98 (t, 12H, $N(CH_2CH_2CH_2C\mathbf{H}_3)_4^+$), 1.39 (h, 8H, $N(CH_2CH_2C\mathbf{H}_2CH_3)_4^+$), 1.57 (m, 8H, $N(CH_2C\mathbf{H}_2CH_2CH_3)_4^+$), 3.14 (t, 8H, $N(C\mathbf{H}_2CH_2CH_2CH_3)_4^+$)), 8.02 (s, 4H, **H**-Ph), 8.87 (s, 1H, **H**C(O)CCN), ppm. ^{13}C NMR ($CDCl_3$, 100 MHz): 13.53, 19.65, 23.81, 58.82, 81.61, 82.66, 119.94, 122.02, 122.86, 123.96, 124.24, 124.48, 126.77, 129.04, 141.10, 141.38. 146.11, 147.18, 176.71 and 177.09 ppm. Melting point: 235-238 ºC. Crystals of **3f** suitable for X-ray diffraction were grown from a dmso/water solution (1:10 v/v) of **3d** in the presence of *n*-Bu_4NOH at room temperature after 45 days.

Physical Techniques. Elemental analysis (C, H and N) were carried out on a Perkin-Elmer 2400 analyzer. Infrared spectra were recorded with Perkin-Elmer FTIR spectrometer as KBr pellets in the 4000-400 cm^{-1} region (Supporting Information, SI, Figures S1-S12). NMR spectra was carried in Bruker-200/300/400 NMR spectrometers at 200, 300 or 400 MHz for ^{1}H nuclei (50, 75 and 100 MHz for ^{13}C) using dmso-d_6 or $CDCl_3$/dmso-d_6 mixture (1:5 v/v) or $CDCl_3$ with c.a. 20 mg

of material. Tetramethylsilane or residual solvent signals were used as internal standard (SI Figures S13-S36). X-ray powder diffraction patterns for compounds **2b**, **3b**, **3d**, **2e** and **3f** were obtained using a Rigaku/Geirgeflex or PANalytical/Empyrean diffractometer at room temperature (SI Figures S37-41). The patterns were compared with the calculated ones from the cif files with the reflection positions based on cell parameters and intensity peaks in both cell parameters and atom positions using the Mercury® software.[26] The observed cell contraction in compounds **2e** and **3f** through the analysis of the single crystal data collection at 120 K account for the major deviation on the reflection positions when compared with the X-ray pattern collected at room temperature. For a realistic comparison, the cell parameters at room temperature of **2e** and **3f** were determined by measuring single crystals at low diffraction limit and compared to the polycrystalline data through the JANA2006[27] software matching all diffraction peaks. Thermogravimetric analysis were carried out for **2b**, **2e** and **3b**. The analysis were performed in a thermobalance Shimadzu TA-60 using nitrogen flow at rate of 50 mL min^{-1} and alumina crucible as sample holder containing 3-6 mg of material (SI Figures S48-S50).

Crystal Data Collection and Refinement. X-ray diffraction data for **2b**, **2e**, **3b**, **3d**, and **3f** were performed with an Oxford-Diffraction GEMINI-Ultra diffractometer using Enhance Source Cu-K_α radiation (λ = 1.5418 Å) or Enhance Source Mo-K_α radiation (λ = 0.71073 Å). Measurements were performed at different temperatures as shown in Table 1. Data integration and scaling of the reflections for all compounds were performed with the *CRYSALIS* suite.[28] Final unit cell parameters were based on the fitting of the positions of all reflections. Analytical absorption corrections were performed by means of the *CRYSALIS* suite and the space group identification was done with *XPREP*.[29] The structures of all compounds were solved by direct methods using the *SUPERFLIP* program.[30,31] For each compound, the positions of all non-hydrogen atoms could be unambiguously assigned on consecutive difference Fourier maps. Refinements were performed using *SHELXL*-2018[32] based on F^2 through full-matrix least-squares routine. All non-hydrogen atoms were refined with anisotropic atomic displacement parameters. The hydrogen atoms were located in difference maps and included as fixed contributions according to the riding model. $U_{iso}(H) = 1.5\ U_{eq}(O)$ for water molecules. The values of C–H and N–H of the organic

moieties were considered equal to 0.97 Å and U_{iso}(H) = 1.2 U_{eq}(C or N) for aromatic carbon atoms, methylene and amide groups.[33] A double split position model was applied to the model disordered *n*-Bu_4N^+ units in **2e**. Molecular graphics were prepared with the ORTEP3-2014 software.[34] CCDC deposit numbers are 1843194 (**2b**), 1843195 (**2e**), 1843196 (**3b**), 1843197 (**3d**) and 1843198 (**3f**).

Table 1. Summary of the crystal data and refinement parameters for **2b**, **2e, 3b**, **3d**, and **3f**.

Compound	**2b**	**2e**	**3b**	**3d**	**3f**
Chemical Formulae	$C_9H_{13}N_3OCl_4Sn$	$C_{54}H_{90}N_8O_7$	$C_{18}H_{18}N_4O_2Cl_6Sn$	$C_{13}H_{12}N_2O_4$	$C_{25}H_{41}N_3O_3$
*F*w / g mol^{-1}	439.71	963.33	653.75	260.25	431.61
λ / Å	1.5418	0.71073	1.5418	0.71073	0.71073
Crystal Size / mm^3	0.40 × 0.11 × 0.01	0.17 × 0.10 × 0.08	0.39 × 0.17 × 0.07	0.16 × 0.14 × 0.13	0.54 × 0.18 × 0.14
Crystal System	Triclinic	Monoclinic	Orthorhombic	Monoclinic	Monoclinic
Space Group	$P\bar{1}$	$P2_1/c$	$Cmce$	$P2_1/c$	$P2_1/n$
a / Å	7.006(5)	17.8761(15)	7.0873(2)	8.4720(11)	11.7417(14)
b / Å	9.684(5)	20.1749(11)	18.2022(6)	20.459(3)	9.6253(15)
c / Å	11.987(5)	31.536(3)	20.2832(7)	7.1990(16)	22.1211(15)
α / º	69.910(5)	90	90	90	90
β / º	89.440(5)	104.661(8)	90	96.958(16)	99.154(8)
γ / º	84.970(5)	90	90	90	90
Volume / Å^3	760.7(7)	11003.0(15)	2616.62(15)	1238.6(4)	2468.2(5)
T / K	150(2)	120(2)	290(2)	298(2)	120(2)

Z (*Z*')	2 (2)	2 (16)	4 (4)	4 (4)	4 (4)
F(000)	428	4208	1288	544	944
hkl range	$-5 \le h \le 8$	$-20 \le h \le 22$	$-24 \le h \le 24$	$-10 \le h \le 10$	$-14 \le h \le 14$
	$-11 \le k \le 11$	$-25 \le k \le 25$	$-21 \le k \le 20$	$-24 \le k \le 25$	$-12 \le k \le 9$
	$-14 \le l \le 14$	$-39 \le l \le 36$	$-8 \le l \le 7$	$-8 \le l \le 8$	$-20 \le l \le 27$
ρ_{calc} / g cm^{-3}	1.920	1.163	1.660	1.396	1.161
μ / mm^{-1}	19.772	0.077	13.601	0.105	0.076
Collected reflections	6229	149679	7457	10667	11620
Independent Reflections	2666	22505	1280	2515	5037
Reflections with $I \ge 2\sigma(I)$	1911	13010	1011	1450	3741
R_{int}	0.122	0.093	0.084	0.078	0.032
R^a; wR^b [$I \ge 2\sigma(I)$]	0.074; 0.170	0.076 (0.136)	0.047 (0.118)	0.052 (0.106)	0.048; 0.103
R^a; wR^b (all data)	0.108; 0.204	0.194 (0.232)	0.063 (0.130)	0.114 (0.141)	0.075; 0.119
Goodness-of-fit on F^2 (S^c)	1.060	1.049	1.052	1.058	1.027
Larg. diff. peak and hole/e Å^{-3}	+1.84; –1.22	+1.50; –0.41	+1.11; –0.68	+0.22; –0.21	+0.32; –0.28

[a] $R = \sum ||F_o| - |F_c|| / \sum |F_o|$. [b] $wR = [\sum w(|F_o|^2 - |F_c|^2)^2 / \sum w|F_o|^2]^{1/2}$. [c] $S = [\sum w(|F_o|^2 - |F_c|^2)^2 / (N_o - N_p)]^{1/2}$ where w is proportional to σ^{-1} whereas N_o and N_p are the number of observed and refined parameters, respectively.

Comments on the Synthesis

Several other preparative routes have been proposed to synthetize azole compounds, the preparation of derivatives followed by the ring close step being easy and common pathways in the literature for 1*H*-pyrazoles,[35-42] but much less explored for isozaxoles.[43-46] The synthesis of the malonaldehyde requires the presence of the Vilsmeier complex which is achieved by using dmf with a chlorination compound, originally[47] and mostly $POCl_3$.[48] However, as described in the present work, we were able to change the chlorinating reagent in the preparation of **1** without compromising the yield. The replacement of $POCl_3$ by $SOCl_2$ is interesting from an economic point of view since the last one is less expensive and wider available than phosphorous(V) oxychloride and in addition, our synthesis is cleaner due to the release of gaseous SO_2 instead of phosphoric acid which is present at the end of reaction with $POCl_3$.

The ring closing step was carried out without any difficulty, simply reacting **1** either with hydrazine (**2a**) or hydroxylamine (**3a**) sulfate with no need of adding a base (see Schemes 1 and 2). Although the products were prepared as crystals, ensuring high purity, their crystal structures could not be determined precluding an even deeper investigation of the hydrogen bonds. Thus, the nitro group reduction was carried out in two ways: (i) by means of tin in a hydrochloric solution and (ii) by using hydrazine associated with palladium on activated carbon. **2a** was successfully reduced using both methods affording **2b** and **2c**, respectively; however, **3a** did not yield the desired product when hydrazine was added to it and only the tin/HCl route was used leading to **3b**. This simple observation was the first evidence that the isoxazole group does not endure basic media and we should carry out the synthesis in acidic or neutral conditions. The use of **2b** to continue the synthetic pathway was found to be tricky. All procedures applied to deprotonate and isolate the amine from the tin byproducts failed and no pure amine was obtained, being the reason to focus on the hydrazine-Pd/C as the main reduction agent and therefore, only **2c** was used in the synthesis. The deprotonation of **3b** and the isolation of **3c** revealed to be easier than in the case of **2b**, simply extracting **3c** from an aqueous carbonate solution with chloroform at room temperature in a high yield. **2c** and **3c** were used to prepare the oxamate-based compounds **2d** and **3d** by applying the classical procedure of the nucleophilic substitution on carbonyl

chloride, a widely explored route in the synthesis of this type of compounds.[49-52] Compound **2d** was efficiently hydrolyzed upon heating its solution in the presence of tetra-*n*-butylammonium hydroxide. The *n*-tetrabutylammonium salt **2e** crystallizes by cooling down the solution. As previously indicated this does not occur with **3d**. The isoxazole group has a quite acid hydrogen atom and once captured, ring opening occurs.[12,53] This parallel reaction competes with the oxamate hydrolysis and complex mixtures are obtained when the basic hydrolysis was attempted. To prove its incompatibility of **3d** with basic solutions, we reacted it with tetra-*n*-butylammonium hydroxide and crystals of **3f** were obtained, showcasing the open ring reaction, but the oxamate was hydrolyzed off and the amine was transformed into the nitro group by oxidation in the open air. **3f** could be also obtained in a larger scale by reacting **3b** or **3e** (its conjugated acid) with *n*-Bu_4NOH.

Description of structures.

Compound 2b. The asymmetric unit of **2b** consists of diprotonated 4-(4-aminophenyl)-1*H*-pyrazole molecules (the aniline and pyrazol free nitrogen atoms being protonated) and the triclorostannate(II) and chloride anions in a 1:1 molar ratio balancing the positive charges (Fig. 1). One water molecule of crystallization is also present. Both N–C and N–N bonds on the pyrazolium group are very similar. Thus, no substantial localization of double bonds is observed, as one can see in Table 2. This fact together with the NMR spectrum corroborate that it is an aromatic group. Some steric hindrance may be found around C7–H7···H5–C5 and C9–H9···H3–C3 type interactions, since a torsion angle of 2.8(5)º is observed. Due to the large C8–C4 bond length [1.512(1) Å], one can conclude that the aromatic systems are not conjugated and further larger torsion angles can be observed in compounds derived from **2b**, since it has very strong single bond character. Additionally, the protonated aniline nitrogen atom to phenyl ring bond length [N1–C1 = 1.473(1) Å] is considerably larger than the predicted value for the aromatic atoms [c.a. 1.39 Å], as a result of its loss of conjugation because of the protonation. Dealing with the anionic tin(II) unit, the metal atom exhibits a pyramidal geometry being surrounded by three chloride ligands with Sn-Cl bond lengths and Cl–Sn–Cl bon angles covering the ranges 2.532(3)-

2.555(4) Å and 88.0(1)-91.5(1)º, respectively. Main geometric parameters for the pyrazolium group and the $[SnCl_3]^-$ entity are listed in Table 2.

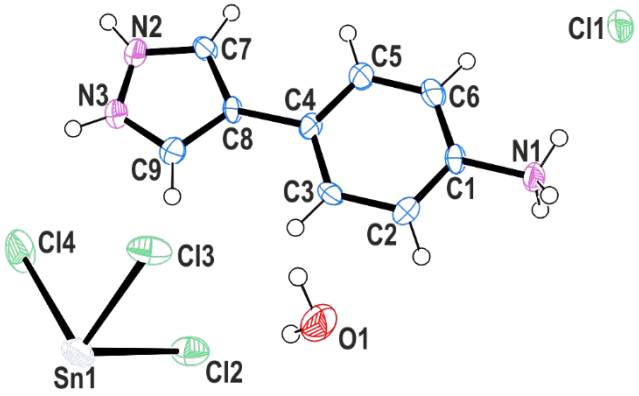

Figure 1. Asymmetric unit of **2b** with the atom numbering. The hydrogen atoms (black circles) were not labeled for the sake of clarity. Thermal ellipsoids are drawn at the 50% of probability level.

Table 2. Selected structural data for the triclorostannate(II) complex anion and the pyrazolium group of **2b**

$[SnCl_3]^-$				Pyrazolium group			
Bond lengths / Å		Cl–Sn–Cl / º		Bond lengths / Å		Angle / º	
Sn1–Cl3	2.532 (3)	Cl3–Sn1–Cl2	88.05 (11)	N2–N3	1.322 (15)	C7–N2–N3	108.3 (9)
Sn1–Cl2	2.554 (3)	Cl3–Sn1–Cl4	91.53 (14)	N2–C7	1.333 (15)	C8–C7–N2	108.1 (10)
Sn1–Cl4	2.555 (4)	Cl2–Sn1–Cl4	89.64 (13)	C7–C8	1.409 (16)	C9–C8–C7	105.2 (10)
				C8–C9	1.399 (18)	N3–C9–C8	106.8 (11)
				C9–N3	1.336 (17)	N2–N3–C9	111.6 (10)

The packing of **2b** is mainly ruled by hydrogen bonds (Table 3). The most remarkable supramolecular structure for this compound is constituted by the free chloride anion and the organic cation. Each chloride anion interacts with a pyrazolium ($N3^i$) and one anilinium (N1) nitrogen atoms with a $N3^i\cdots Cl1\cdots N1$ angle of 106.9(3)º, leading to a supramolecular chain that is extended by translation of the motifs $N1\cdots Cl1^i = 3.242(9)$ Å and $N3\cdots Cl1^i = 3.184(9)$ Å [symmetry code: (i) = x, y, $-1+z$ and (ii) = x, $-1+y$, z]. This trend is near to inversion center resulting in a

View Article Online
DOI: 10.1039/C9CE00215D

double chain, with a ladder-like conformation, connected by hydrogen bond between the anilinium group and a nearest chloride anion in an apical position, as pictured in Figure 2 [N1···Cl1^{iii} = 3.206(9) Å; symmetry code: (iii) = 1–*x*, 2–*y*, –*z*].

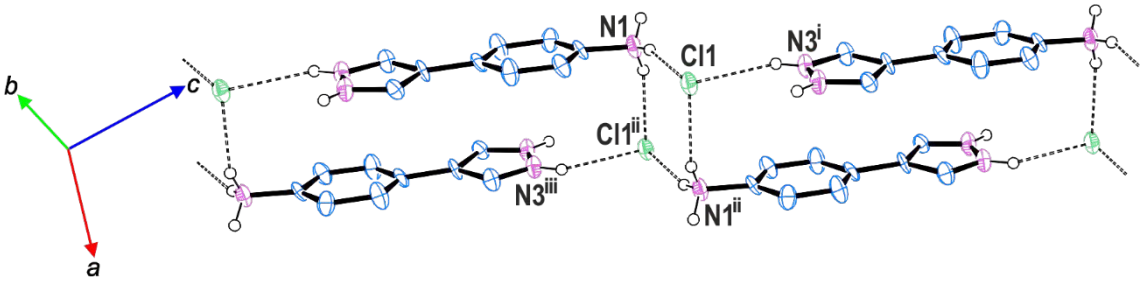

Figure 2. Ladder-like supramolecular chain of **2b** trough N-H···Cl hydrogen bonds. All hydrogen atoms, except those bonded to nitrogen atoms, crystallization water molecule and $[SnCl_3]^-$ units were omitted for clarity.

Hydrogen bonds also occur involving the other pyrazolium protonated nitrogen atom (N2), the water molecule (O1) and trichlorostannate(II) anion (via Cl2, Cl3 and Cl4 atoms). These groups are responsible for the interconnection of the double chains in the crystallographic *bc* plane trough the pyrazolium-water hydrogen bond [N2–H2···O1^{iv}; (iv) = *x*, *y*–1, *z*], followed by the water–$[SnCl_3]^-$ interaction [O1–H*W*2···Cl3] and by the [SnCl3]$^-$–anilinium contact [N3–H3···Cl4] from the subsequent set of chains (see Table 3 and Figures S42 and S43). Finally, the supramolecular chains are packed along the crystallographic *a* axis by π–π stacking between the pyrazolium and phenyl rings, the values of their geometric center separation being 3.67(1) Å within each double ladder-like chain and 3.97(1) Å between adjacent double chains.

Table 3. Hydrogen bond parameters of **2b***

D–H···A	D–H / Å	H···A / Å	D···A / Å	D–H···A / º
N1–H1*B*···Cl1^{i}	0.89	2.37	3.244 (10)	166
N1–H1*C*···Cl1^{ii}	0.89	2.38	3.205 (11)	154
N1–H1*A*···Cl4^{iii}	0.89	2.94	3.231 (10)	100

View Article Online
DOI: 10.1039/C9CE00215D

N2–H2···O1^{iv}	0.86	1.84	2.674 (12)	164
N3–H3···Cl4	0.86	2.71	3.305 (11)	128
N3–H3···Cl1^{iv}	0.86	2.52	3.189 (10)	136
O1–H*W*2···Cl3	0.90	2.57	3.220 (7)	130
O1–H*W*1···Cl2	0.90	2.42	3.276 (6)	160

*Symmetry codes: (i) = *x*, *y*, *z*–1; (ii) = –*x*+1, –*y*+2, -*z*; (iii) = *x*, *y*+1, *z*-1; iv = *x*, *y*–1, *z*.

Compound 3b. The isoxazole derivative **3b** is a salt made up by two 4-(isoxazol-4-yl)anilinium cations and one hexachlorostannate(IV) anion (Figure 3). It crystallizes in the centrosymmetric orthorhombic *Cmce* space group. Due to the planarity of the cationic organic moiety all its non-hydrogen atoms are placed over a mirror symmetry element, meanwile the tin atoms occupy the inversion center positions.

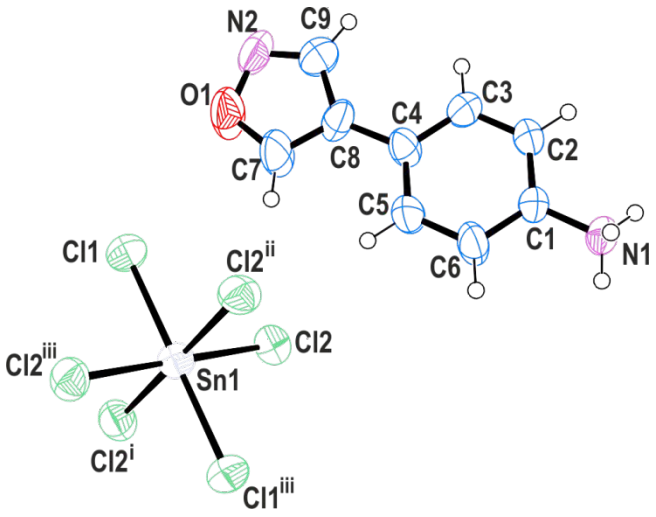

Figure 3. View of asymmetric unit of **3b** with the atom numbering. The symmetry operation over the tin atom was applied to visualize the whole hexachlorostannate(IV) anion in order to get a better understanding of the structure. The hydrogen atoms (black circles) were not labeled for the sake of clarity. Thermal ellipsoids are drawn at the 50% of probability level [Symmetry code: (i) = –*x*, *y*, *z*; (ii) = *x*, –*y*, 1–*z*; (iii) = –*x*, –*y*, 1–*z*]

The isoxazole group in **3b** revealed to be an aromatic system, as confirmed by ^{1}H NMR and ^{13}C chemical shifts but differently of **2b**, there is a major localization of the double bonds in **3b**. The C–O bond length is 1.333(11) Å against 1.297(14) Å for the C–N bond. This difference is also observed in the C–C bond distances [1.351(14) and 1.408(12) Å for C7–C8 and C8–C9, respectively]. The organic moiety of this compound is monoprotonated, the aniline part being the only one to be protonated under our synthetic conditions (pK_a of anilinium is 4.7 whereas that of the isoxazolium is –2.3).[54] Just as found in **2b**, steric hindrance [C7–H7···H5–C5 and C9–H9···H3–C3] combined with the high single bond characteristics of the inter-ring link [C4–C8 = 1.469(11) Å] conclude in a torsion angle of aromatic rings of 7(2)º. Somewhat the major localization of the double bonds in **3b** cause the aromatic rings to be more conjugated, since the C4–C8 bond in this case is shorter than in **2b**. The metal center in the hexachlorostannate(IV) complex anion is in an almost perfect octahedral geometry, as expected for a cation with the [Xe]$5d^0$ electronic configuration. The Sn–Cl bond lengths and the Cl–Sn–Cl angles cover the ranges 2.424(1) [Sn1–Cl2] to 2.431(1) Å [Sn1–Cl2] and 89.15(7)-90.85(7)º respectively (see Table 4 for more details about these parameters).

Table 4. Main structural parameters of the hexachlorostanate(IV) anion and and isoxazole group in **3b***

$[SnCl_6]^{2-}$				Isoxazole group			
Bond lengths / Å		Cl–Sn–Cl / º		Bond lengths / Å		Angles / º	
Sn1–Cl1	2.431 (1)	Cl1–Sn1–Cl1^{i}	180	N2–O1	1.389 (16)	C9–N2–O1	104.7 (11)
Sn1–Cl2	2.424 (1)	Cl1–Sn1–Cl2	90.33 (5)	N2–C9	1.27 (2)	C7–O1–N2	108.6 (10)
		Cl1–Sn1–Cl2^{i}	90.33 (5)	O1–C7	1.330 (17)	N2–C9–C8	114.1 (13)
		Cl1–Sn1–Cl2^{ii}	89.67 (5)	C7–C8	1.345 (19)	C7–C8–C9	101.7 (12)
		Cl1–Sn1–Cl2^{iii}	89.67 (5)	C8–C9	1.412 (18)	O1–C7–C8	110.9 (12)
		Cl2–Sn1–Cl2^{i}	90.85 (7)				
		Cl2–Sn1–Cl2^{ii}	89.15 (7)				

View Article Online
DOI: 10.1039/C9CE00215D

Cl2–Sn1–Cl2^{iii}	180	

*Symmetry codes: (i) = $-x$, y, z; (ii) = x, $-y$, $1-z$; (iii) = $-x$, $-y$, $1-z$.

Once more, the crystal packing is dictated by the hydrogen bonds and C–H···O type interactions. A self-recognition of the cations is observed along the crystallographic *b* axis. In these molecules, the isoxazole nitrogen atom is recognized by the anilinium group [N1···N2^{iv} = 2.894(10) Å; (iv) = $-x$, $-1/2+y$, $1/2-z$]. It repeats indefinably leading to a supramolecular chain (Figure 4). The isoxazole oxygen atom weakly interacts with one phenyl C–H group [C2···O1^{iv} = 3.307(10) Å]. The other two anilinium hydrogen atoms also establish weak interactions with two different $[SnCl_6]^{-}$ groups, one above and other below the main plane of this cation, interconnecting the chains (see Table 5 and Figures S44 and S45). The chains are also packed down the crystallographic *c* axis via isoxazole π–π stacking [a separation of 3.57(1) Å between the centroids of the rings being observed through this interaction].

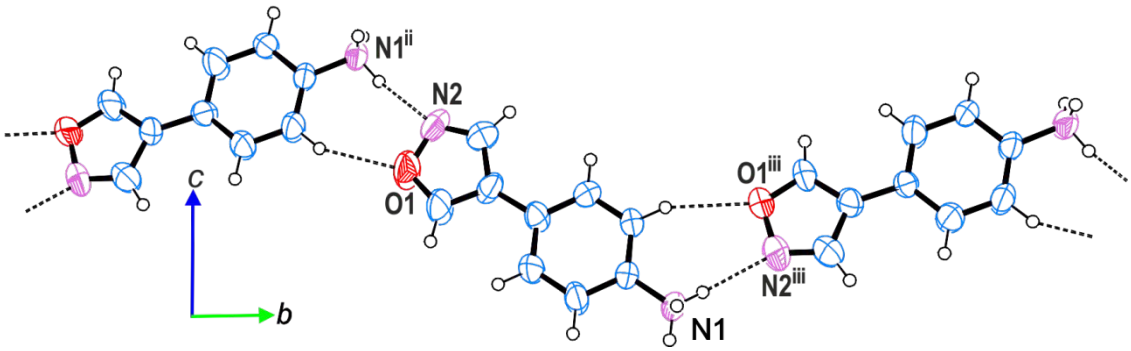

Figure 4. Supramolecular zigzag chain in **3b** with cation-cation anilinium-isoxazol self-reorganization trough N–H···N hydrogen bonds and C–H···O type interactions (dotted lines). Atomic color scheme follows that in Figure 3.

Table 5. Intermolecular interactions of **3b***

D–H···*A*	D–H / Å	H···A / Å	D···A / Å	D–H···A / º
N1—H1*B*···N2^{iv}	0.89	2.50	2.894 (10)	108

View Article Online
DOI: 10.1039/C9CE00215D

C2—H2···O1^{iv}	0.93	2.43	3.307 (10)	156
N1—H1*C*···Cl1^{v}	0.89	2.88	3.5445 (2)	133
N1—H1*C*···Cl2^{v}	0.89	2.86	3.424 (6)	123
N1—H1*A*···Cl2^{vi}	0.89	2.75	3.465 (6)	139
N1—H1*B*···Cl2^{vii}	0.89	2.86	3.424 (6)	123
N1—H1*B*···Cl1^{vii}	0.89	2.88	3.5445 (2)	133
N1—H1*A*···Cl2^{viii}	0.89	2.75	3.465 (6)	139

* Symmetry codes: (iv) = –*x*, –1/2+*y*, 1/2–*z*; (v) = 1/2+*x*, –1/2–*y*, 1–*z*; (vi) = 1/2+*x*, –1/2+*y*, *z*; (vii) = –1/2–*x*, –1/2–*y*, 1–*z*; (viii) = –1/2–*x*, –1/2+*y*, *z*.

Compound 2e. The asymmetric unit of the organic salt **2e** is constituted by four independent anionic oxamic derivatives 4-(1*H*-pyrazol-4-yl)phenyl-*N*-oxamate), four tetra-n-butylamonium cations and two water molecules of crystallization (Figure 5). Although all anions are chemically identical, the torsion angle of the aromatic rings in the solid state vary together with the angle of the terminal methyl group of the cations (Figure S46). The pyrazole groups in **2e** are deprotonated in contrast with **2b**. However, they remain very symmetrical looking at the C–N bonds, revealing that the asymmetrical presence of the hydrogen atom is not a fundamental factor to interfere on the aromaticity, and consequently, on the bond lengths. Details of the geometry of the pyrazole groups and the deviation of the planarity of the rings and the oxamate planes are shown in Table 6.

View Article Online
DOI: 10.1039/C9CE00215D

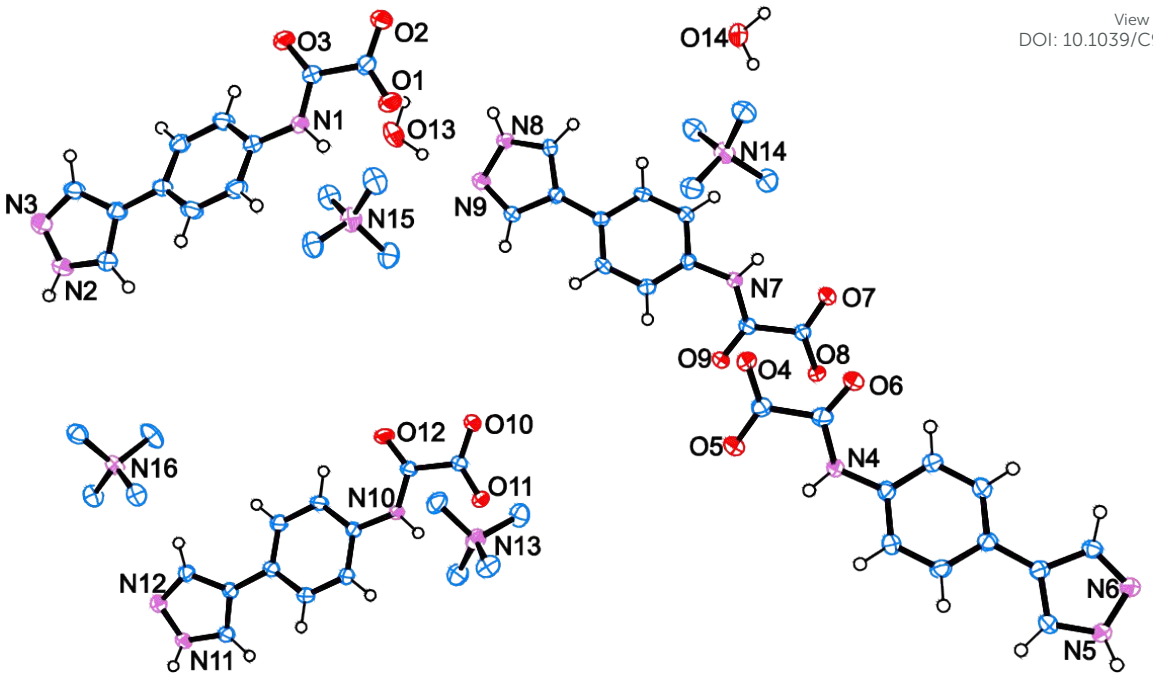

Figure 5. Asymmetric unit of **2e** with the atom numbering. The terminal $-(CH_2)_2CH_3$ and hydrogen atoms of *n*-Bu_4N cations were omitted for clarity. All remaining carbon atoms (blue ellipsoids) and hydrogen atoms (black circles) were not labeled. Thermal ellipsoids are drawn at the 50% of probability level.

The result of this large asymmetric unit is a crystal packing formed by layers of hydrophobic and hydrophilic interactions very well separated and packed along the crystallographic *c* axis (Figure S47). Each hydrophobic layer contains only tetra-*n*-butylammonium cations whereas the 4-(1*H*-pyrazole-4-yl)phenylene-*N*-oxamate anions and the crystallization water molecules constitute each hydrophilic layer. The hydrogen bonds are the main interaction observed within the hydrophilic layer, forming a 2D network as shown in Figure 6. There are three different interaction motifs (black dotted lines in Figure 6): (i) the protonated pyrazole-nitrogen atom that recognizes the carboxylate part of the oxamate group in the first one; (ii) the second one concerns the double oxamate amide-to-carboxylate supramolecular dimer; (iii) and the water molecule that connects the deprotonated pyrazole-nitrogen atom and the carboxylate groups in the third one. Finally, other very weak C-H···O and C-H···N type interactions may be pointed out, where aromatic hydrogen atoms are very close to hydrogen bond acceptors.

View Article Online
DOI: 10.1039/C9CE00215D

In this respect, a dimeric interaction concerning the pyrazole groups where the carbon bonded to the deprotonated nitrogen atom approaches significantly to the nearest pyrazole nitrogen atom occurs (golden dotted lines in Figure 6). Also, one of the phenyl hydrogen atoms is very close to the carboxylate oxygen atom involved in the double oxamate interaction (see the green dotted lines in Figure 6). This interaction may be responsible for the deviations of the torsion angles, since it is not observed in all crystallographically independent anions. The supramolecular interactions in **2e** are displayed in Figure 6 and the list of the hydrogen bonds in this compound is given in Table 7.

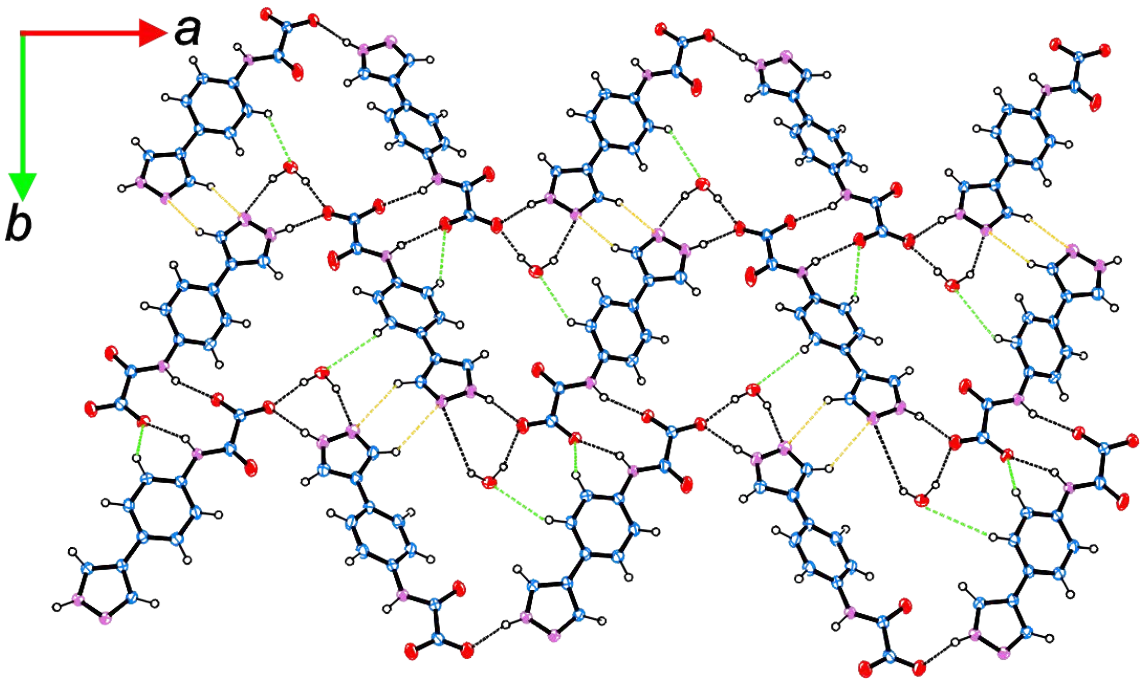

Figure 6. View of a fragment of the supramolecular 2D hydrogen network (black dot lines) in **3e** featuring the pyrazole-oxamate and oxamate-oxamate self-reorganization of the anion motifs, mediated by crystallization water molecule. Additional very weak interactions involving aromatic carbon atoms as hydrogen donors are displayed interacting with oxygen (lime green dot lines) and non-protonated pyrazole nitrogen atoms (golden dot lines).

Table 6. Bond lengths in the pyrazole rings and their torsion angles in relation to the phenyl and oxamate mean planes for each crystallographically independent $HPyox^-$ anion in **2e**

Ring **A**[£]		Ring **B**[£]		Ring **C**[£]		Ring **D**[£]	
Bond Lengths / Å							
N2–N3	1.346(3)	N5–N6	1.345(3)	N8–N9	1.353(3)	N11–N12	1.345(3)
C9–N2	1.327(4)	C20–N5	1.335(3)	C31–N8	1.334(3)	C42–N11	1.342(3)
C9–C10	1.378(4)	C20–C21	1.370(4)	C31–C32	1.371(4)	C42–C43	1.371(4)
C10–C11	1.396(4)	C21–C22	1.400(4)	C32–C33	1.409(4)	C43–C44	1.405(4)
C11–N3	1.326(4)	C22–N6	1.326(3)	C33–N9	1.329(3)	C44–N12	1.325(3)
Torsion angle in relation to the phenyl ring							
28.5(7)º		17.6(7)º		14.2(6)º		24.2(5)º	
Torsion angle in relation to the oxamate mean plane							
1.3(5)º		5.0(5)º		9.7(4)º		12.6(3)º	

[£]The ring label is according to the concerned nitrogen atoms: **A**, **B**, **C** and **D** rings contain the N2/N3, N5/N6, N8/N9 and N11/N12 pairs, respectively.

Table 7. Summary of the hydrogen bonds in **2e***

D—H···A	D—H	H···A	D···A	D—H···A
O14—H14*A*···N12^{i}	0.93	2.01	2.900 (3)	160
O14—H14*B*···O8^{ii}	0.92	2.01	2.890 (3)	158
O13—H13*B*···N9	1.02	2.03	3.028 (3)	164
O13—H13*A*···O10^{iii}	0.97	1.97	2.815 (3)	144
N8—H8*A*···O10^{iii}	0.88	1.91	2.776 (3)	167
N8—H8*A*···O12^{iii}	0.88	2.48	2.990 (3)	117
N1—H1···O5^{iv}	0.88	2.05	2.881 (3)	157
N2—H2···O4^{v}	0.88	1.88	2.755 (3)	173
N4—H4*A*···O1^{vi}	0.88	2.11	2.923 (3)	152
N5—H5*A*···O2^{vii}	0.88	1.88	2.745 (3)	166
N5—H5*A*···O3^{vii}	0.88	2.47	2.978 (3)	117
N7—H7*A*···O7^{ii}	0.88	2.27	3.080 (3)	152
N10—H10···O11^{viii}	0.88	2.16	2.982 (3)	156
N11—H11*A*···O8^{viii}	0.88	1.89	2.755 (3)	166
N11—H11*A*···O8^{viii}	0.88	1.89	2.755 (3)	166

*Symmetry code: (i) = *x*+1, *y*–1, *z*; (ii) = –*x*+1, –*y*, –*z*; (iii) = –*x*+1, –*y*+1, -*z*; (iv) = –*x*+1, *y*+1/2,

View Article Online
DOI: 10.1039/C9CE00215D

$-z+1/2$; (v) = x, $y+1$, z; (vi) = $-x+1$, $y-1/2$, $-z+1/2$; (vii) = $x-1$, $y-1$, z; (viii) = $-x$, $-y+1$, $-z$.

Compound 3d. The oxamate derivative of the isoxazole based molecule 4-(1,2-oxazol-4-yl)phenylene-*N*-(ethyloxamate) crystallizes in the centrosymmetric monoclinic $P2_1/c$ space group. It is a neutral unit with no solvent molecules of crystallization. This compound is built up by an isozaxole group linked to a phenyl ring which has an oxamate fragment in its *para* position, as displayed in Figure 7. Intriguingly, the isoxazole ring in **3d** has highly delocalized double bonds with very close values of the C9–N2 and C7–O1 bonds [1.302(3) and 1.339(3) Å, respectively], as well as the carbon-carbon bonds with less discrepancy than that observed in the related compound **3b**. Although **3d** seems to have the most conjugated rings of all azol compounds herein, the combination of the aromatic hydrogen steric hindrance [C7–H7···H5–C5 and C9–H9···H3–C3] and van der Waals forces combined lead this compound to have the greatest torsion angle between the aromatic mean planes [11.1(5)º]. The torsion angle between the isoxazole ring and the oxamate mean plane [calculated for the N1O2O3O4C10C11 set of atoms] is equal to 4.7(5)º, and the dihedral angle between the oxamate and phenyl ring is 10.4(5)º.

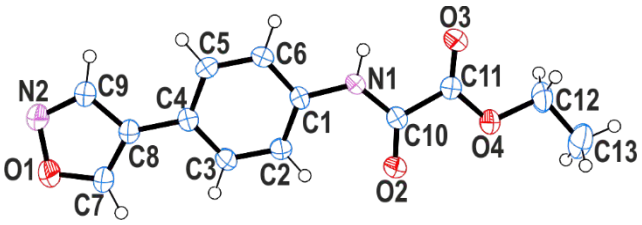

Figure 7. Asymmetric unit of **3d** with the atom numbering. The hydrogen atoms (black circles) were not labeled for clarity. Thermal ellipsoids are drawn at the 50% probability level.

Hydrogen bonds are occur in the crystal packing of **3d** (see Figure 8). The absence of charges in this compound changes de molecular recognition drastically compared to what was observed in **2e**. The only hydrogen bond donor in **3d** (the amide-oxamate group), recognizes the isoxazole nitrogen atom [N1···N2^{i} = 3.067(3) Å; (i) = $x-1$, $-y+1/2$, $z-1/2$]. This hydrogen bond net grows along the crystallographic *a* axis leading to a supramolecular chain. Additional very

weak C-H···O type interactions can be found in this crystal packing involving the aromatic hydrogen atoms interacting with the carbonyl oxygen atoms [C5–H5···O3^{ii} and C7–H7···O3^{ii}; (ii) = x+1, –y+1/2, z+1/2] and the isoxazole one [C2–H2···O1^{i}] (lime and orange dotted lines in Figure 8). They connect the supramolecular chains allowing the growth of the crystal into two directions. Finally, van der Waals contacts are found dealing with the ester aliphatic part and phenyl rings, both parallel and perpendicular to the crystallographic *ab* plane resulting in a 3D supramolecular network and crystal formation. A summary of the interactions in **3d** is shown in Table 8.

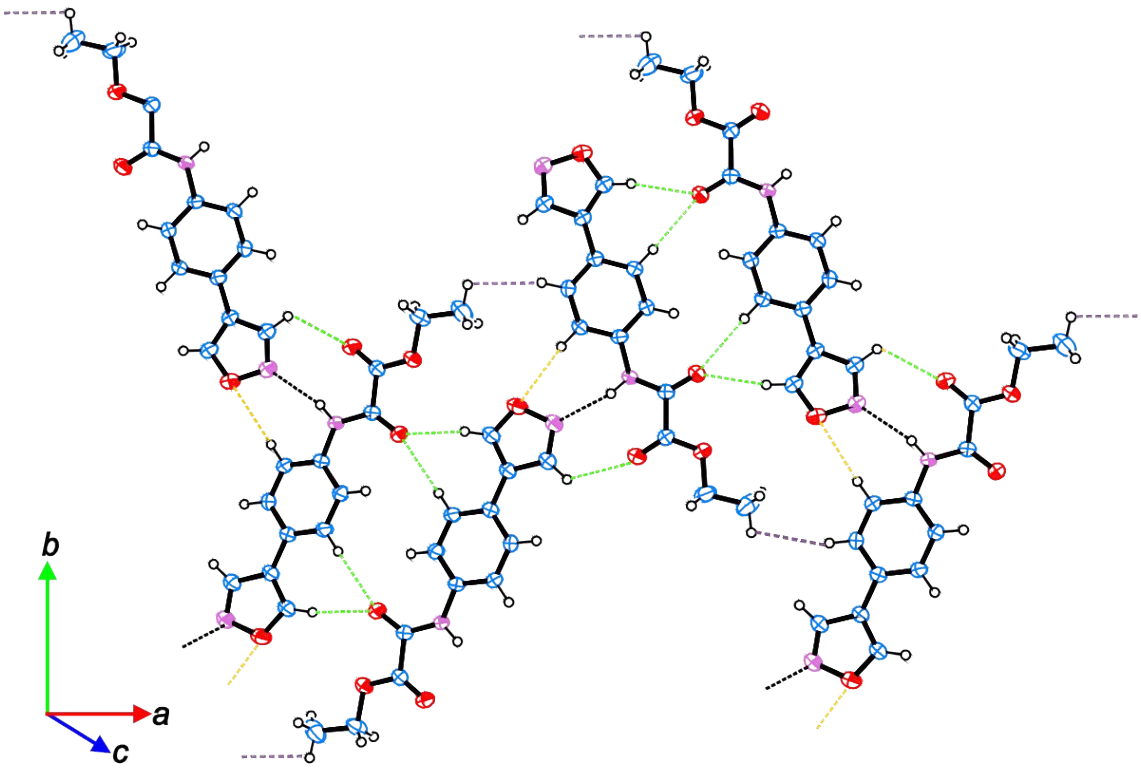

Figure 8. View of a fragment of the supramolecular 2D network in **3d** featuring the N–H···N oxamate-isoxazole self-reorganization of the motifs. Additional very weak C–H···N and C–H···N type interactions involving aromatic C–H donors interacting with carbonyl groups (lime green dot lines) and isoxazol oxygen atoms (orange dotted lines) are also displayed. Interactions between the methyl and aromatic C–H groups are featured as purple dotted lines.

Table 8. Supramolecular interactions in **3d***

View Article Online
DOI: 10.1039/C9CE00215D

D—H···A	D—H	H···A	D···A	D—H···A
N1—H1···N2^{i}	0.86	2.23	3.067 (3)	165
C2—H2···O1^{i}	0.93	2.63	3.506 (3)	158
C5—H5···O3^{ii}	0.93	2.46	3.379(2)	168
C7—H7···O3^{ii}	0.93	2.53	3.085 (3)	119
C9—H9···O2^{iii}	0.93	2.39	3.299 (3)	167
C3—H3···C13^{iv}	0.93	3.04	3.830 (3)	144

*Symmetry code: (i) = *x*–1, –*y*+1/2, *z*–1/2; (ii) = *x*+1, –*y*+1/2, *z*+1/2; (iii) = –*x*+3, –*y*+1, –*z*+1; (iv) = –*x*+2, *y*–1/2, –*z*+1/2.

Compound 3f. This compound is the result of the cleavage of the isoxazole derivative in basic media, the tetra-n-butylammonium cation balancing its negative charge. It crystallizes in the centrosymmetric monoclinic $P2_1/n$ space group and the anion is a *para* disubstituted nitrobenzene with a carbon atom (C8) bonded to a formyl and a nitrile groups (See Figure 9). Although the negative charge of the organic anion is mainly located on this C8 atom, it is somewhat delocalized on the adjacent C4, C7 and C9 carbon atoms. In this respect, whereas the bond lengths C7–O3 = 1.223(2) Å and C9–N2 = 1.150(2) Å for formyl and nitrile groups, compare well those of the sp^3 carbon in acetaldehyde (*c.a.* 1.22 Å)[56-58] and acetonitrile (1.17 Å)[59-61] supporting the no conjugation, the values of the carbon-carbon bonds indicate the opposite, being shorter than in the model molecules [C7–C8 = 1.412(2) Å, C8–C9 = 1.413(2) Å and C8–C4 = 1.441(2) Å, in comparison with acetaldehyde,[55-57] acetonitrile[58-60] and toluene[58-60] where the bond lengths are 1.50, 1.46 and 1.55 Å, respectively]. Additionally, the X-ray powder diffraction patterns proves the bulk material to have the same structure than that of the single crystals, meanwhile NMR spectra suggests mixture of different contents, which may be due to resonance structures with enough large lifetimes to be detected separately. The crystal packing is dictated by van der Waals interactions and the ions form segregated layers of cations and anions along the crystallographic *c* axis (see Figure 10).

View Article Online
DOI: 10.1039/C9CE00215D

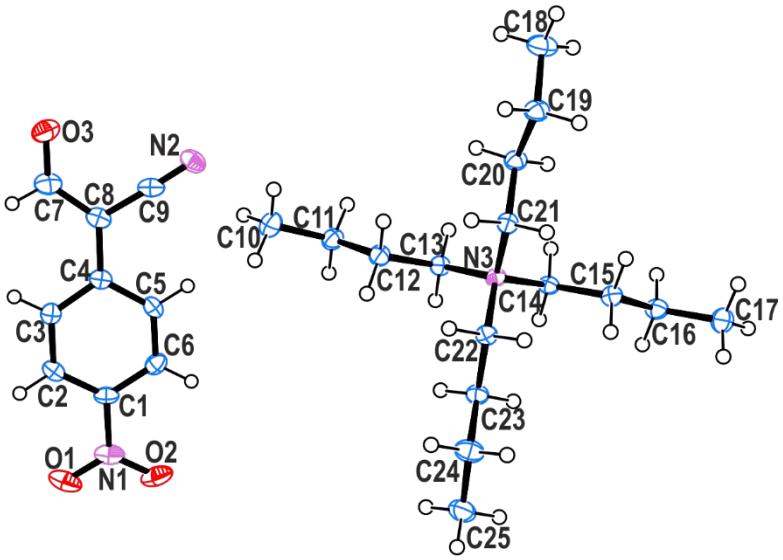

Figure 9. View of the asymmetric unit of **3f** with the atom numbering. The hydrogen atoms (black circles) were not labeled for clarity. Thermal ellipsoids are drawn at the 50% of probability level.

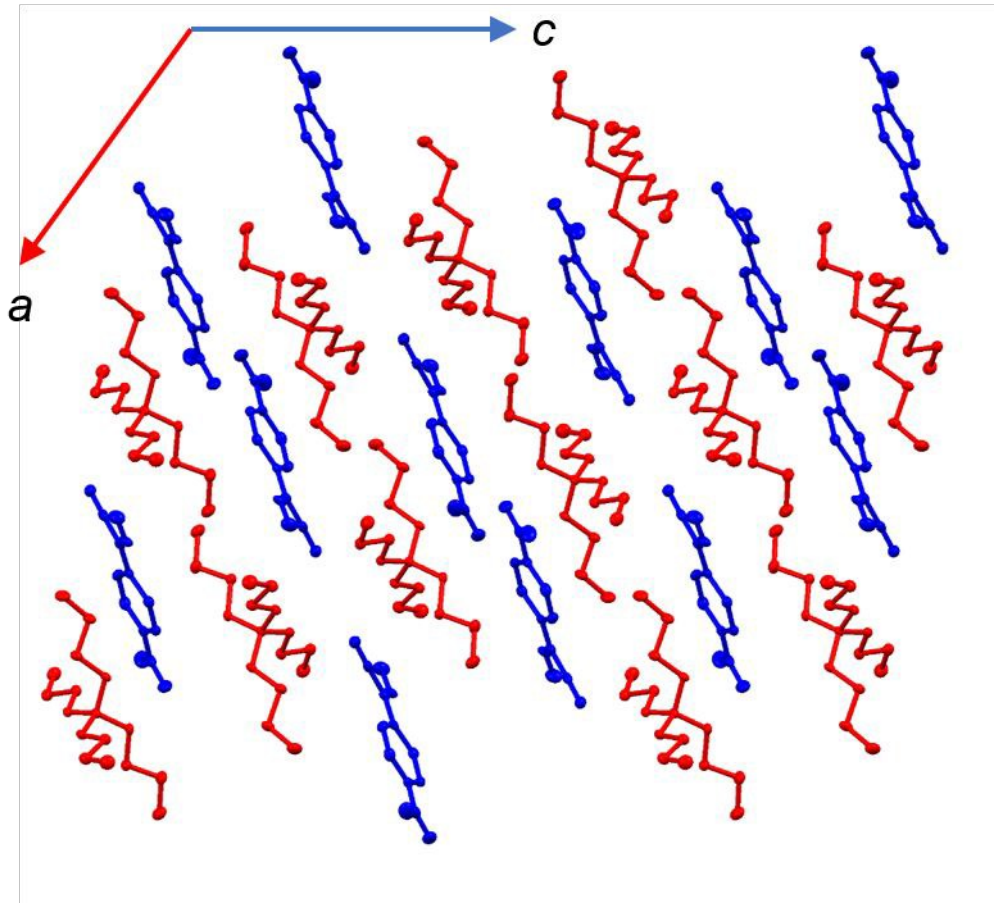

Figure S10 – Crystal packing of **3f** down the crystallographic *b* axis featuring the hydrophobic cationic (red) and hydrophilic anionic (blue) layers in an alternated stacking.

View Article Online
DOI: 10.1039/C9CE00215D

Comparison and correlations of the hydrogen bonds

Let us to compare the hydrogen bonds of the X-ray structures of the work into two ways: firstly, we will compare the pyrazole-based molecules **2b** and **2e** and isoxazole **3b** and **3d** pairs separately and secondly, the similar molecules replacing pyrazole by an isoxazole will be discussed, that is **2b** with **3b** and **2e** with **3d**.

The pyrazole group in **2b** is protonated and it seeks the larger concentration of negative charges, which in this case are on the free chloride ion and on the water molecules, while the charge in the $[SnCl_3]^-$ unit is spread over all its atoms. Additionally, one can see that all hydrogen bond donors in the 4-(4-ammoniophenyl)-1*H*-pyrazol-2-ium cations have at least one interaction with the free chloride anion. A deeper analysis of the crystal structure of **2e** indicate the center of all hydrogen bonds are also the negative charge, in this case centered on the carboxylate groups. Since stronger hydrogen bonds occur with more negatively charged acceptor atoms, there is no competition for other kind of recognition besides negatively charged groups in both cases. Interestingly, the supramolecular dimeric interactions of the oxamate groups remain in **2e** even though when more hydrogen bond acceptors and donors are present, this feature revealing a very stabilizing motif for further solid state studies and crystal packing predictions with oxamate derivatives. So, in the presence of negatively charged groups, the pyrazole-based molecules tend to recognize them instead of themselves.

The anilinium group in **3b** is the only hydrogen bond donor, since the isoxazole molecules/groups are poor bases, corroborated in this case because in concentrated HCl solution the isozaxole ring was ineffective to become protonated. But even being a poor base, the lone pair of its nitrogen atom, which is out of the ring current, is the most available negative charge in this compound. The isoxazole-oxygen atom is not a good hydrogen bond acceptor being a very electronegative atom– aromatic sp^2 atom bonded to a high electronegative one – and the charge is less available in $[SnCl_6]^{2-}$ since the high positive charge on the metal center [Sn(IV)] turns the chloride ligands not so good hydrogen bond acceptors. Thus, in **3b** one can see the molecular recognition of isoxazole groups by the anilinium in **3b** and therefore, we can conclude that the 4-

(4-ammoniophenyl)-1,2-oxazole cations are able to recognize themselves in this compound. Among all possible hydrogen acceptors in **3d**, the isoxazole nitrogen atom is still the better choice since it is the less electronegative, even being a poor base. Then, the neutral oxamate group can recognize the isoxazole and 4-(1,2-oxazole-4-yl)phenylene-*N*-(ethyloxamate) molecules recognize themselves. This molecular recognition has proved to be stronger than the supramolecular dimeric interaction of the oxamate fragments in the neutral units and this motif predominates in the lack of additional hydrogen bond donors.

Among the anilinium molecules, we can conclude the pyrazol-based one (**2b**) showcases a lack of possibility to self-recognition. The pyrazolium group is less acidic than the anilinium one. In other words, anilinium groups will not find hydrogen bond acceptors in the pyrazole groups at same chemical environment and/or pH value. That is the opposite of **3b** and we can extend this fact to other similar isoxazole-based anilinium compounds. Because of their very low pK_a values, there is a large pH window to work with and keep the hydrogen bond acceptor for the anilinium group. Dealing with the phenyloxamate-based molecules, we can conclude that the pyrazol tends to recognize the oxamate especially when it is negatively charged, but when it is not, the isoxazole showed to be a better hydrogen aceptor than any carbonyl group. One can also extend the tendency to neutral phenyloxamate molecules to recognize the pyrazole group, since it is a better base than the isoxazole.

Conclusions

In this work we provided a new synthetic route for 2-(4-nitrophenyl)-1,3-propanedial (**1**) by replacing $POCl_3$ by $SOCl_2$ and then explored the synthetic pathways of pyrazol- (**2a-2e**) and isoxazole-substituted (**3a-3d**) phenyloxamate molecules, all the steps in high yield and purity. Most of them have been prepared as crystalline powders or single crystals (**2b**, **2e**, **3b**, **3d** and **3f**). We have also evidenced the incompatibility of the isoxazole groups with basic solutions (**3f**). The crystal structure of isolated compounds investigated herein revealed some trends concerning the hydrogen bond behavior in the solid state. The pyrazole fragments in neutral or positively charged forms are very good hydrogen bonds donors and seek the hydrogen acceptor group or atom with

the highest amount of negative charge, such was the chloride anion (**2b**) and the carboxylate group (**2e**), which were recognized by the pyrazole groups. The lack of a hydrogen bond donor character in the isoxazole group turns it a good acceptor in comparison with the coordinated chloride ligands (**3b**) and the carbonyl group of the ester and amide (**3d**), leading to self-recognition in both cases. Extrapolations could be made for the pyrazole groups. For instance, the deprotonated nitrogen atom in neutral molecules can be hydrogen bond acceptor as good as the isoxazole and probably will self-recognize its molecules.

Acknowledgements

This work was supported by Conselho Nacional de Desenvolvimento Científico e Tecnológico (CNPq) (Projects 405199/2016-3 and 308836/2015-4), Fundação de Amparo à Pesquisa do Estado de Minas Gerais (FAPEMIG) (Project PPM-00508-16), Coordenação de Aperfeiçoamento de Pessoal de Nível Superior (CAPES) (Finance Code 001), Ministerio Español the Economía y Competitividad (Projects CTQ2016-75068P and Unidad de Excelencia María de Maetzu MDM2015-0538), Centre Nationale de la Recherche Scientifique (CNRS) (PICS07345 Spanish-French project), the CAPES/ COFECUB (Ph-C 856-15 Brazilian-French project).

References

1. H.-J Schneider. Binding Mechanisms in Supramolecular Complexes. *Angew. Chem. Int. Ed.*, 2009, **48**, 3924-3977.

2. E. Persch, O. Dumele, F. Diederich. Molecular Recognition in Chemical and Biological Systems. *Angew. Chem. Int. Ed.*, 2015, **54**, 3290-3327.

3. J. A. A. W. Elemans, S. Lei, S. de Feyter. Molecular and supramolecular networks on surfaces: from two-dimensional crystal engineering to reactivity. *Angew. Chem. Int. Ed.*, 2009, **48**, 7298-7332.

4. D. L. Nelson, M. M. Cox. *Lehninger Principles of Biochemistry*; W. H. Freeman & Co.: London, 2013; pp 1-300.

5. Q. Liu, J. Wang, B. J. Boyd. Peptide-based biosensors. *Talanta*, 2013, **136**, 114-127.

6. Z. T. Ball. Molecular recognition in protein modification with rhodium metallopeptides. *Curr. Opin. Chem. Biol*., 2015, **25**, 98-102.

7. J.-M. Lehn, M. Mascal, A. DeCian, J. Fischer. Molecular ribbons from molecular recognition directed self-assembly of self-complementary molecular components. *J. Chem. Soc. Perkin Trans. 2*, 1992, **0**, 461-467.

8. D. B. Amabilino, D. Williams, J. F. Stoddart. From Solid-State Structures and Superstructures to Self-Assembly Processes. *Chem. Mater*. 1994, **6**, 1159-1167.

9. M. P. Suh, Y. E. Cheon, E. Y. Lee. Syntheses and functions of porous metallosupramolecular networks. *Coord. Chem. Rev.*, 2008, **252**, 1007-1026.

10. T. Friščić. Supramolecular concepts and new techniques in mechanochemistry: cocrystals, cages, rotaxanes, open metal–organic frameworks. *Chem. Soc. Rev*., 2012, **41**, 3493-3510.

11. W. Yang, Y. Li, H. Liu, L. Chi, Y. Li. Design and assembly of rotaxane-based molecular switches and machines. *Small*, 2012, **8**, 504-516.

12. J. Alvarez-Builla, J. J. Vaquero, J. Barluenga. *Modern Heterocyclic Chemistry*, Wiley-VCH Verlag: Weinheim, 2011; pp 635-808.

13. R. K. Bansal, *Heterocyclic Chemistry*, New Age International: New Delhi, 1999; pp 389-440.

14. U. P. Singh, S. Narang. A supramolecular approach towards the construction of molecular salts using phosphonic acid and pyrazole. *CrystEngComm*, 2014, **16**, 7777-7789.

15. M. L. Gallego, M. Cano, J. A. Campo, J. V. Heras, E. Pinilla, M. R. Torres. Supramolecular Arrays of Cationic Complexes Containing Pyrazole Ligands and Tetrafluoroborate, Trifluoromethanesulfonate, or Nitrate as Counterions. Crystal Structure of Bis(3,5-dimethyl-4-nitro-1*H*-pyrazole-κN^2)silver(1+) Nitrate ([Ag(Hpz^{NO2})$_2$](NO_3)). *Helv. Chim. Acta*, 2005, **88**, 2433-2440.

16. S. Moyano, J. Barberá, B. E. Diosdado, J. L. Serrano, A. Elduque, R. Giménez. Self-assembly of 4-aryl-1H-pyrazoles as a novel platform for luminescent supramolecular columnar liquid crystals. *J. Mater. Chem. C*, 2013, **1**, 3119-3128.

17. C. Obuah, A. Munyaneza, I. A. Guzei, J. Darkwa, Ferrocenylpyrazolyl palladium complexes as catalysts for the polymerisation of 1-heptene and 1-octene to highly branched polyolefins. *Dalton Trans.*, 2014, **43**, 8940-8950.

18. M. Tang, W. Zhang, Y. Kong, DABCO-promoted synthesis of pyrazoles from tosylhydrazones and nitroalkenes. *Org. Biomol. Chem*., 2013, **11**, 6250-6254.

19. C. D. Mboyi, C. Duhayon, Y. Canac, R. Chauvin. From *N*-sulfonyl,*C*-homoallyl-hydrazones to pyrazole and pyridazine (N_2)-heterocycles: the ultimate aromatization process. *Tetrahedron*, 2014, **70**, 4957-4968.

20. F.-G. Zhang, Y. Wei, Y.-P. Yi, J. Nie, J.-A. Ma. Regioselective Cycloaddition of Trifluorodiazoethane with Electron-Deficient Allenic Esters and Ketones: Access to CF_3-Substituted Pyrazolines and Pyrazoles. *Org. Lett*., 2014, **16**, 3122-3125.

21. D. K. Kim, E. A. Shokova, V. A. Tafeenko, V. V. Kovalev. Synthesis of 1,3-diketones from 3-(4-R-phenyl)propionic acids. *Russ. J. Org. Chem*., 2014, **50**, 464-468.

22. W.-S. Yu, C.-C. Cheng, Y.-M. Heng, P.-C. Wu, Y.-H. Song, Y. Chi, P.-T. Chou. Excited-State Intramolecular Proton Transfer in Five-Membered Hydrogen-Bonding Systems: 2-Pyridyl Pyrazoles. *J. Am. Chem. Soc*., 2003, **125**, 10800-10801.

23. G. D. Frey, W. W. Schoeller, E. Herdtweck. Solid-state and Calculated Electronic Structure of 4-Acetylpyrazole. *Z. Naturforsch. B: Chem. Sci.*, 2014, **69**, 839-843.

24. H. McNab, I. Clelland, S. Parsons, D. Messenger. Private Communication: CCDC code CARXOJ, 2005.

25. F. Crestey, S. Stiebing, R. Legay, V. Collot, S. Rault. Design and synthesis of a new indazole library: direct conversion of N-methoxy-N-methylamides (Weinreb amides) to 3-keto and 3-formylindazoles. *Tetrahedron*, 2007, **63**, 419-428.

26. C. F. Macrae, P. R. Edgington, P. McCabe, E. Pidcock, G. P. Shields, R. Taylor, M. Towler, J. van de Streek. Mercury: visualization and analysis of crystal structures. *J. Appl. Cryst*. 2006, **39**, 453-457

27. V. Petricek, M. Dusek, L. Palatinus. Crystallographic Computing System JANA2006: General features. *Z. Kristallogr*. 2014, **229**, 345-352.

28. CrysAlisPRO. Rigaku Oxford Diffraction: Yarnton, Oxfordshire, England, 2018.

29. Sheldrick, G. M. XPREP. Bruker-AXS, Madison, Wisconsin, USA, 2001.

30. L. Palatinusz, G. Chapuis. SUPERFLIP – a computer program for the solution of crystal structures by charge flipping in arbitrary dimensions *J. Appl. Cryst*., 2007, **40**, 786-790.

31. L. Platinus, S. J. Prathapa, S. van Smaalen. EDMA: a computer program for topological analysis of discrete electron densities. *J. Appl. Cryst*., 2012, **45**, 575-580.

32. G. M. Sheldrick, Crystal structure refinement with SHELXL. *Acta Crystallogr. Sect. C*, 2015, **71**, 3-8.

33. C. K. Johnson. *Crystallographic Computing,* Ahmed, F.; Hall, S. R.; Huber, C. P., Eds.; Munksgaard; Copenhagen, 1970, pp 207-220.

34. H. D. Flack, U. Shmueli. The mean-square Friedel intensity difference in P1 with a centrosymmetric substructure. *Acta Cryst*., 2007, **A63**, 257-265.

34. L. J. Farrugia. WinGX and ORTEP for Windows: an update. *J. Appl. Cryst.*, 2012, **45**, 849–854.

35. V. Král, L. Jelínek, S. Šaman . Preparation and synthetic utilization of diarylmethylenemalonaldehydes. *Collect. Czech. Chem. Commun*., 1989, **54**, 2721-2730.

36. K. N. Zelenin, A. R. Tugusheva, S. I. Yakimovich, V. V. Alekseev, E. V. Zerova. 5-Hydroxy-2-pyrazolines and Some of Their 1-Substituted Analogs. *Chem. Heterocycl. Compd*., 2002, **38**, 668-676.

37. H. Gnichtel, U. Boehringer. Die Beckmann-Reaktion bei phenylsubstituierten 1,3-Dioximen. *Ber*., 1980, **0**, 1507-1513.

38. W. Adam, M. Diedering, Enhanced formation of inverted housane through steric effects by rotationally unsymmetric bridgehead substituents in the ring closure of triplet cyclopentane-1,3-diyl diradicals, generated photolytically from 2,3-diazabicyclo[2.2.1]heptene(DBH)-type azoalkanes. *Photochem. Photobiol. Sci*., 2003, **2**, 393-397.

39. W. Adam, T. Heidenfelder, C. Sahin. Diastereo- and Regioselective Synthesis of Diquinanes and Related Systems from Tricyclo[3.3.0.02,4]octanes by Chemical Electron Transfer (CET). *Synthesis*, 1995, **9**, 1163-1170.

40. J. Stephanidou-Stephanatou, Oxidation of bis-aroylhydrazones of 3,3-dimethylpentane-2,4-dione and thermal decomposition of the oxidation products. *J. Heterocycl. Chem.*, 1983, **20**, 845-853.

41. J. E. Baldwin, O. W. Lever, N. R. Tzodikov. Reactions of Methoxyvinyllithium. Synthesis and Rearrangement of 4-Hydroxyisopyrazoles. *J. Org. Chem*., 1976, **41**, 2874-2877.

42. A. L. Baumstark, A. Choudhary, P. C. Vasquez , M. Dotrong. Synthesis of 4,4-dimethyl-3,4-dihydro-3,3,5-trisubstituted-2H-pyrazoles and N-benzoyl derivatives: Method for "Hydrolysis" of unreactive amides and carbamates. *J. Heterocycl. Chem.*, 1990, **27**, 219-294.

43. J. T. Bagdanoff; M. S. Donoviel; A. Nouraldeen,; M. Carlsen, T. C. Jessop, J. Tarver, S. Aleem, L. Dong, H. Zhang, L. Boteju, J. Hazelwood, J. Yan, M. Bednarz, S. Layek, I. B. Owusu, S. Gopinathan, L. Moran, Z. Lai, J. Kramer, S. D. Kimball, P. Yalamanchili, W. E. Heydorn, K. S. Frazier, B. Brooks, P. Brown, A. Wilson, W. K. Sonnenburg, A. Main, K. G. Carson, T. Oravecz, D. J. Augeri. Inhibition of Sphingosine 1-Phosphate Lyase for the Treatment of Rheumatoid Arthritis: Discovery of (E)-1-(4-((1R,2S,3R)-1,2,3,4-Tetrahydroxybutyl)-1H-imidazol-2-yl)ethanone Oxime (LX2931) and (1R,2S,3R)-1-(2-(Isoxazol-3-yl)-1H-imidazol-4-yl)butane-1,2,3,4-tetraol (LX2932). *J. Med. Chem*., 2010, **53**, 8650–8662.

44. M. Moccia, M. Cortigiani, C. Monasterolo, F. Torri, C. D. Fiandra, G. Fuller, B. Kelly, M. F. A. Adamo. Development and Scale-up of an Organocatalytic Enantioselective Process to Manufacture (S)-Pregabalin. *Org. Process Res. Dev*., 2015, **19**, 1274–1281.

45. A. M. Rodriguez, A. Juan, M. V. Gómez, A. Moreno, A. Hoz. Continuous-Flow Microliter Microwave Irradiation in the Synthesis of Isoxazole Derivatives: An Optimization Procedure. *Synthesis*, 2012, **44**, 2527-2530.

46. R. L. Sahani, R.-S. Liu, Development of Gold-catalyzed [4+1] and [2+2+1]/[4+2] Annulations between Propiolate Derivatives and Isoxazoles, *Angew. Chem. Int. Ed*., 2017, **56**, 1026-1030.

47. A. Vieslmeier, A. Haack. Über die Einwirkung von Halogenphosphor auf Alkyl-formanilide. Eine neue Methode zur Darstellung sekundärer und tertiärer *p*-Alkylamino-benzaldehyde. *Ber*., 1927, **60**, 119-122

48. O. Meth-Cohn, S. P. Stanforth. *Comprehensive Organic Synthesis*: The Vilsmeier–Haack Reaction, Pergamon: Oxford, 1991, pp 777-794.

49. F. J. Martínez-Martínez, I. I. Padilla-Martínez, M. A. Brito, E. D. Geniz, R. C. Rojas, J. B. R. Saavaedra, H. Höpfl, M. Tlahuextl, R. Contreras. Three-center intramolecular hydrogen bonding in oxamide derivatives. NMR and X-ray diffraction. *J. Chem. Soc., Perkins Trans. 2* 1998, **0**, 401-406;

50. E. V. García-Bàez, C. Z. Gómez-Castro, H. Höpfl, F. J. Martínez-Martínez. Ethyl *N*-phenyloxamate Acta Cryst. 2003, C59, o541-o543; I. I: Padilla-Martínez, M. Chaparro-Huerta, F. J. Martínez-Martínez, H. Höpfl, E. V. García-Báez. Diethyl *N,N'-m*-phenylenedioxamidate. *Acta Cryst*. 2003, **E59**, o825-o827.

51. I. Yavari, M. Bayat. New Synthesis of Highly Functionalized 3-Pyrrolin-2-Ones. *Synth. Commun.*, 2002, **32**, 2527-2534.

52. H. O. Stumpf. L. Ouahab. A Molecular-Based Magnet with a Fully Interlocked Three-Dimensional Structure. *Science*, 1993, **261**, 447-449.

53. A. De Munno, V. Bertini, F. Lucchesini. On the base catalysed ring opening of 3-unsubstituted isoxazoles. Derivatives of 4- and 5-phenylisoxazole. *J. Chem. Soc., Perkin Trans. 2*, 1977, **0**, 1121-1124.

54. M. Marín-Luna, I. Alkorta, J. Elgueroa. A theoretical study of the gas phase (proton affinity) and aqueous (pK_a) basicity of a series of 150 pyrazoles. *New J. Chem.*, 2015, **39**, 2861-2871.

55. Y.-L. Ren, Y.-W. Zhou, Y.-H. Ye. Structural Study on NMR and X-Ray of Lactucopicrin A Guaianolide Ester. *Struct. Chem*., 2003, **14**, 581-585.

56. A. A. Danopoulos, J. R. Galsworthy, M. L. H. Green, S. Cafferkey, L. H. Doerrer, M. B. Hursthouse. Equilibria in the $B(C_6F_5)_3$–H_2O system: synthesis and crystal structures of $H_2O{\cdot}B(C_6F_5)_3$ and the anions $[HOB(C_6F_5)_3]_-$ and $[(F_5C_6)_3B(\mu\text{-}OH)B(C_6F_5)_3]^-$. *Chem. Commun*. 1998, **0**, 2529-2560.

57. N. Auner, J.-U. Steinberger, B. Herrschaft. Carbon=Carbon Hydrogenation of Silicon-Functionalized Silaheterocycles. *Eur. J. Inorg. Chem*. 1999, **0**, 1095-1102.

58. O. P. Lam, C. Anthon, F. W. Heinemann, J. M. O'Connor, K. Meyer. Structural and Spectroscopic Characterization of a Charge-Separated Uranium Benzophenone Ketyl Radical Complex. *J. Am. Chem. Soc*., 2008, **130**, 6567–6576.

59. M. Berville, L. Karmazin, J. A. Wytko, J. Weiss. Viologen cyclophanes: redox controlled host–guest interactions. *Chem. Commun*., 2015, **51**, 15772-15775.

60. C. Fischer, T. Gruber, D. Eissmann, W. Seichter, E. Weber. Unusual Behavior of a Calix[4]arene Featuring the Coexistence of Basic Cone and 1,2-Alternate Conformations in a Solvated Crystal. *Cryst. Growth Des*., 2011, **11**, 1989–1994.

TOC

View Article Online
DOI: 10.1039/C9CE00215D

Molecular recognition agents in the control of hydrogen bond networks in pyrazole and isoxazole rings.